



Article

Quantitative Estimation of the Impacts of Precursor Emissions on Surface O₃ and PM_{2.5} Collaborative Pollution in Three Typical Regions of China via Multi-Task Learning

Mengnan Liu ¹, Mingliang Ma ^{1,*}, Mengjiao Liu ¹, Fei Meng ¹, Pingjie Fu ¹, Huaqiao Xing ¹, Jingxue Bi ¹, Zhe Zheng ² and Yongqiang Lv ^{1,*}

¹ School of Surveying and Geo-Informatics, Shandong Jianzhu University, Jinan 250101, China; 2022165123@stu.sdjzu.edu.cn (M.L.); 2023165107@stu.sdjzu.edu.cn (M.L.); lzhmf@sdjzu.edu.cn (F.M.); fupingjie19@sdjzu.edu.cn (P.F.); xinghuaqiao18@sdjzu.edu.cn (H.X.); bijingxue19@sdjzu.edu.cn (J.B.)

² Disaster Reduction Center of Shandong Province, Jinan 250102, China; zhengze@shandong.cn

* Correspondence: mamingliang19@sdjzu.edu.cn (M.M.); lvyongqiang19@sdjzu.edu.cn (Y.L.)

Abstract: The coordinated control of PM_{2.5} and O₃ pollution has become a critical factor restricting the improvement of air quality in China. In this work, precursors and related influencing factors were utilized to establish PM_{2.5} and O₃ estimation models in the North China Plain (NCP), the Yangzi River Delta (YRD), and the Pearl River Delta (PRD) using a multi-task-learning (MTL) model. The prediction accuracy of these three MTL models was high, with R² values ranging from 0.69 to 0.83. Subsequently, these MTL models were used to quantitatively reveal the relative importance of each factor to PM_{2.5} and O₃ collaborative pollution simultaneously. Precursors and meteorological factors were the two most critical influencing factors for PM_{2.5} and O₃ pollution in three regions, with their relative importance values larger than 29.99% and 15.89%, respectively. Furthermore, these models were used to reveal the response of PM_{2.5} and O₃ to each precursor in each region. In the NCP and the YRD, the two most important precursors of PM_{2.5} pollution are SO₂ and HCHO, while the two most critical factors for O₃ pollution are HCHO and NO₂. Therefore, SO₂ and VOC emissions reduction is the most important measure for PM_{2.5} pollution, while VOC and NO₂ emission reduction is the most critical measure for O₃ pollution in these two regions. In terms of the PRD, SO₂ and NO₂ are the most important precursors of PM_{2.5} pollution, while the most important precursors for O₃ pollution are HCHO and SO_X, respectively. Thus, NO₂, SO₂, and VOC emission reduction is the most critical measure for PM_{2.5} pollution, while VOC and NO₂ emission reduction is the most critical measure for O₃ pollution in the PRD. Overall, this study provides clues and references for the control of PM_{2.5} and O₃ collaborative pollution in the NCP, the YRD, and the PRD.

Keywords: O₃ pollution; PM_{2.5} pollution; multi-task learning; air quality management



Citation: Liu, M.; Ma, M.; Liu, M.; Meng, F.; Fu, P.; Xing, H.; Bi, J.; Zheng, Z.; Lv, Y. Quantitative Estimation of the Impacts of Precursor Emissions on Surface O₃ and PM_{2.5} Collaborative Pollution in Three Typical Regions of China via Multi-Task Learning. *Sustainability* **2024**, *16*, 2475. <https://doi.org/10.3390/su16062475>

Academic Editors: Giovanni Gualtieri and Enrico Ferrero

Received: 25 January 2024

Revised: 4 March 2024

Accepted: 14 March 2024

Published: 16 March 2024



Copyright: © 2024 by the authors. Licensee MDPI, Basel, Switzerland. This article is an open access article distributed under the terms and conditions of the Creative Commons Attribution (CC BY) license (<https://creativecommons.org/licenses/by/4.0/>).

1. Introduction

Nowadays, air pollution has become the most important environmental problem in the world [1–4], and for China, PM_{2.5} and O₃ are the two main air pollutants restricting the improvement of air quality in China [5,6]. PM_{2.5} pollution harms human health and ecosystems and affects climate change [7,8]. Previous studies have shown that PM_{2.5} pollution increases the risk of lower respiratory infections (LRIs) [9], coronary heart disease (CHD) [10], and stroke [11] in humans. In addition, PM_{2.5} is one of the major causes of hazy weather [12], and can lead to reduced visibility [8]. In order to effectively improve air quality, the Air Pollution Prevention and Control Action Plan (APAP) has been promoted by the government since 2013. Subsequently, PM_{2.5} pollution levels in China have improved significantly after 2013 [13,14], while O₃ pollution level has risen significantly and the area affected by O₃ pollution has expanded significantly in recent years [1,15–18]. O₃ pollution adversely affects crop growth [19,20], ecosystems [21,22], and human health by causing

cardiovascular diseases in humans [23,24] and other issues. Furthermore, human health and ecosystem gains from reduced PM_{2.5} pollution are offset by increased O₃ pollution [25], especially in densely populated and economically developed regions such as the North China Plain (NCP), the Yangtze River Delta (YRD), and the Pearl River Delta (PRD) [21,26]. Therefore, it is necessary to reveal the main controlling factors behind PM_{2.5} and O₃ collaborative pollution, and to propose corresponding measures.

There are similarities and differences between reducing air pollution caused by PM_{2.5} and O₃. O₃ and the secondary components in PM_{2.5} are both produced by atmospheric chemical reactions, and they have similar precursors including NO_x and VOC. However, the response of O₃ pollution to reductions in NO_x and VOC emissions is different from that of PM_{2.5} pollution. In addition, the emission reduction in ozone precursors should be in accordance with local conditions and the corresponding proportion; unreasonable emission reduction may lead to the exacerbation of O₃ pollution [27]. For example, reductions in NO_x and VOC reduce PM_{2.5} pollution levels, but in the NO_x-sensitivity regime, the reduction in NO_x significantly reduces O₃ pollution levels, and the reduction in VOC leads to an increase in O₃ pollution levels. In contrast, in the VOC-sensitivity regime, the reduction in VOC would significantly reduce O₃ pollution levels, but the reduction in NO_x would result in an increase in O₃ pollution levels [12,28].

Therefore, exploring the contribution and impact of PM_{2.5} and O₃ precursor emissions on PM_{2.5} and O₃ collaborative pollution simultaneously can help to formulate synergistic emission reduction strategies for PM_{2.5} and O₃ precursors to be able to control PM_{2.5} and O₃ collaborative pollution in a better way. However, most previous studies only explored the impacts of the influencing factors on PM_{2.5} pollution [29] or O₃ pollution [15,16,30], while there are fewer studies revealing the effects and contributions of the influencing factors on PM_{2.5} and O₃ collaborative pollution simultaneously [31–33]. Few previous studies that simultaneously reveal the influence and contribution of influencing factors to the synergistic pollution of PM_{2.5} and O₃ mainly use atmospheric chemistry models, and the accuracy of the models needs to be improved [32,33]. In addition, the few studies that have used statistical modelling to reveal the influence and contribution of influencing factors to PM_{2.5} and O₃ collaborative pollution have mainly considered meteorological [10] and precursor [34–36] factors. However, these statistical models are not able to estimate and reveal the contribution of the same factor to both PM_{2.5} and O₃ simultaneously, and more than one model needs to be built to estimate and reveal the contribution of a particular factor to both PM_{2.5} and O₃ [35,36].

In this work, to better control PM_{2.5} and O₃ collaborative pollution, the impacts of precursors emissions, meteorological factors, population density, the normalized difference vegetation index (NDVI), land use and land cover (LULC), and other influencing factors of PM_{2.5} and O₃ collaborative pollution are assessed comprehensively. Three regions, including the NCP, the PRD, and the YRD, which generate more than 36% of GDP (Gross Domestic Product) of China [37], and are the three most densely populated regions in China, were selected as our study areas. Daily gridded PM_{2.5} and O₃ (maximum daily 8 h average ozone, MDA8) datasets from 2010 to 2020, daily gridded SO₂ and NO₂ datasets, daily gridded Aerosol Optical Depth (AOD) products, NDVI datasets observed by Moderate Resolution Imaging Spectroradiometer (MODIS), meteorological reanalysis datasets, aerosol component dataset (AC), PM_{2.5} and O₃ precursor reanalysis datasets, population density, and LULC datasets of China were utilized to establish the PM_{2.5} and O₃ estimation model using a multi-task learning (MTL) model. Subsequently, the same PM_{2.5} and O₃ estimation MTL model of each region (including the NCP, the PRD and the YRD) was used to quantitatively reveal the relative importance of each factor to PM_{2.5} and O₃ collaborative pollution simultaneously, and the most critical influencing factors of PM_{2.5} and O₃ pollution in three regions were revealed. Furthermore, the PM_{2.5} and O₃ estimation MTL model was used to quantitatively reveal the response of PM_{2.5} and O₃ to each precursor simultaneously, as well as the domain precursor pollutants of PM_{2.5} and O₃ collaborative pollution in the NCP, the PRD and the YRD.

2. Data

2.1. Surface PM_{2.5} and O₃ Estimation Products

In this study, a daily 1 km × 1 km resolution gridded PM_{2.5} concentration dataset derived from the Long-Term Gap-Free High-Resolution Air Pollutant concentration dataset (LGHAP) [14] (Bai et al., 2022) from 2010 to 2020 was utilized as one learning target of the surface O₃ and PM_{2.5} estimation MTL model. In addition, daily aerosol optical depth (AOD) data derived from this LGHAP dataset during 2010 and 2020 were also utilized as an influencing factor for PM_{2.5} pollution. Subsequently, PM_{2.5} and AOD datasets were also uniformly resampled and up-scaled to 0.1° for spatiotemporal matching with other model input datasets. In addition, the daily gridded gap-free surface O₃ concentration dataset (0.1° × 0.1°) from 2010 to 2020 derived from our previous study by Ma et al. (2023) [17] was also used as another learning target of the surface O₃ and PM_{2.5} estimation MTL model. In this work, daily gridded surface PM_{2.5} and O₃ concentration datasets were considered as the surface measurements for PM_{2.5} and O₃ pollution and were used as the modeling targets for the surface O₃ and PM_{2.5} estimation MTL models. For more details of the LGHAP dataset and gap-free O₃ concentration dataset, please refer to Bai et al. (2022) [14] and Ma et al. (2023) [17].

2.2. Precursor Factors

To reveal the impact of precursor emissions on PM_{2.5} and O₃ collaborative pollution, precursor factor datasets including SO_X, NO_X, VOC, aerosol component, HCHO column density, surface SO₂, and surface NO₂ were used in this study to estimate the impact of precursors on PM_{2.5} and O₃ collaborative pollution. Similar with surface O₃, daily gridded (0.1° × 0.1°) gap-free surface SO₂ and surface NO₂ datasets from 2010 to 2020 were also derived from our previous study [17]. Moreover, monthly SO_X and NO_X anthropogenic emission inventories (0.1° × 0.1°) were obtained from the Copernicus Atmosphere Monitoring Service (CAMS) atmospheric reanalysis datasets. Due to the absence of available measurement datasets for VOC, 3 h CAMS reanalysis datasets (0.75° × 0.75°) for hydrogen peroxide (H₂O₂), methane (CH₄), isoprene (C₅H₈), peroxyacetyl nitrate (PAN), hydroxyl radical (OH), and propane (C₃H₈) were utilized as proxy datasets for VOC. However, there were a large number of VOC, so using only the six VOC mentioned above instead of all VOC would result in incomplete information on VOC, and it is widely believed that HCHO is a by-product of the oxidation process of many VOC, so the CAMS daily formaldehyde (HCHO) reanalysis data were also used here as an important proxy for VOC. In addition, hourly aerosol component datasets (0.5° × 0.625°) including black carbon surface mass (BCSM), dust surface mass density of PM_{2.5} (DUSMASS25), and organic carbon surface mass (OCSM) derived from the Modern-Era Retrospective analysis for Research and Applications version 2 (MERRA-2) were used in this work as influencing factors for PM_{2.5} pollution. MERRA-2 is the latest version of global atmospheric reanalysis for the satellite era produced by NASA Global Modeling and Assimilation Office (GMAO) using the Goddard Earth Observing System Model (GEOS). Finally, precursor factor datasets were resampled to 0.1° for spatiotemporal matching with other model input datasets before they were input into the PM_{2.5} and O₃ estimation MTL model.

2.3. Meteorological Factors

In addition to precursor emission factors, PM_{2.5} and O₃ collaborative pollution is also governed by meteorological factors, and, therefore, a range of meteorological factors were utilized to establish the PM_{2.5} and O₃ estimation MTL models. Hourly meteorological datasets (0.1° × 0.1°) including surface UV radiation (UV), surface 2 m temperature (T), boundary layer height (BLH), wind speed (WS), wind direction (WD), relative humidity at 1000 hpa (RH), surface pressure (SP), total precipitation (TP), and total cloud cover (TCC) derived from the fifth generation ECMWF reanalysis for the global climate and weather reanalysis (ERA5) between 2010 and 2020 were utilized to establish the PM_{2.5} and O₃ estimation MTL models. Subsequently, daily accumulated UV and TP, daily averaged

RH, SP, BLH, and TCC, daily maximum T, and hourly values of WS and WD at 14:00 p.m. (at which the highest MDA8 and temperature is oftentimes observed) were extracted and utilized in the PM_{2.5} and O₃ estimation MTL models [17].

2.4. Auxiliary Data

In addition to precursors and meteorological factors, auxiliary factors including population density, NDVI, AOD, land use and land cover datasets were utilized to establish the PM_{2.5} and O₃ estimation MTL models. Annual gridded population density (1 km × 1 km) derived from the China Resource and Environmental Science Data Center (CRESDC) (Beijing, China) was resampled to 0.1° × 0.1° for spatiotemporal matching with other model input datasets. In addition, Yang and Huang (2021) [38] provided annual LULC datasets for China, where LULC1 to LULC9 denote cropland, forests, shrubs, grasslands, watersheds, snow and ice, wasteland, impervious surfaces, and wetlands, respectively. Moreover, NDVI datasets derived from the 16-day product of MODIS with a grid resolution of 0.05° × 0.05° and daily AOD were two other influencing factors used in the PM_{2.5} and O₃ estimation MTL models. Finally, these auxiliary factor datasets were resampled to 0.1° for spatiotemporal matching with other input datasets before modelling. All datasets utilized in this work were summarized in Table S1.

3. Methods

3.1. Multi-Task Learning Modelling

As an extension of traditional statistical modelling, machine learning methods, due to their excellent performance, have been widely used for air pollutant estimation modelling in recent years [15,17,39,40]. However, these machine learning models are not able to estimate and reveal the contribution of the same factor to both PM_{2.5} and O₃ simultaneously, and more than one model needs to be built to estimate and reveal the contribution of a particular factor to both PM_{2.5} and O₃. Therefore, the multi-task learning (MTL) model was applied to this study to simulate both PM_{2.5} and O₃ pollution in the same model and to reveal the impact and contribution of each factor on PM_{2.5} and O₃ pollution simultaneously. Multi-task learning, known as inductive transfer or inductive bias learning, describes the joint learning of multiple related tasks so that the knowledge contained in one task can be utilized by the others, thus improving generalization of the model [41–43]. The hidden layer of the MTL model consists of two parts: the shared layer and the split layer [44]. The shared layer can learn from all tasks and capture the intrinsic features of the data. The split layer can use latent features learnt from previous layers to learn task-specific information. The model can share information between different tasks and be specialized for individual tasks by sharing and splitting in layers [45]. The model can be represented simply as

$$PM_{2.5}, O_3 \sim f(VOCs, \text{Aerosol component}, NO_X, HCHO, SO_X, NO_2, SO_2, AOD, LULC1, LULC2, \\ LULC3, LULC4, LULC5, LULC7, LULC8, LULC9, BLH, RH, SP, T, TCC, TP, UV, WD, \\ WS, NDVI, POPU, Month) \quad (1)$$

where PM_{2.5} and O₃ denote the target time series of the MTL models in each region. SO₂ and NO₂ are daily gridded surface SO₂ and NO₂ estimation products. SO_X and NO_X are monthly gridded CAMS total anthropogenic emissions. HCHO is the daily formaldehyde from CMAS reanalysis data, while VOC represent six kinds of CAMS reanalysis Volatile Organic Compounds, including Hydrogen peroxide (H₂O₂), Isoprene (C₅H₈), Peroxyacetyl nitrate (PAN), Hydroxyl radicals (OH), Methane (CH₄), and Propane (C₃H₈). In addition, aerosol component represents three kinds of a mainly primary aerosol composition, including Black Carbon Surface Mass (BCSM), Dust Surface Mass Density of PM_{2.5} (DUS-MASS25), and Organic Carbon Surface Mass (OCSM) derived from the MERRA-2 datasets. The explanation of other variables can be found in Section 2.

To quantitatively evaluate the influence and contribution of each factor to the PM_{2.5} and O₃ collaborative pollution in the NCP, the YRD, and the PRD, and further quantitatively estimate the response of PM_{2.5} and O₃ collaborative pollution of each region to each

precursor factor, MTL estimation models between the PM_{2.5} and O₃ and their influencing factors for the NCP, the YRD, and the PRD were first established. Subsequently, PM_{2.5} and O₃ MTL estimation models for these three regions were utilized to quantitatively estimate the contribution and impact of each factor to PM_{2.5} and O₃ collaborative pollution in that corresponding region, and to quantitatively evaluate the responses of PM_{2.5} and O₃ collaborative pollution to each precursor factor in that corresponding region. To establish the PM_{2.5} and O₃ MTL estimation models for the NCP, the YRD, and the PRD, precursor emissions, meteorological factors, population density, AOD, NDVI, LULC, and other PM_{2.5} and O₃-influencing factors were first resampled to $0.1^\circ \times 0.1^\circ$ for spatiotemporal matching with other model input datasets before they were input into the PM_{2.5} and O₃ estimation MTL model. Among these datasets, PM_{2.5} and O₃ datasets in these three regions were considered as the target variables of the PM_{2.5} and O₃ estimation MTL models, while the other influencing factors were used as model input-dependent variables. Taking the MTL modelling in North China as an example, daily surface MDA8 and surface PM_{2.5} concentrations and related influencing factors for the corresponding location and date were matched into a single data pair, with all pairs for the NCP including all datasets between 2010 and 2020. Considering that the input sample size of the MTL models of NCP is too large (58,827,538 data pairs), the model input samples were temporally resampled and spatially resampled to reduce the sample size of the model input datasets. For temporal resampling, data pairs from 2010, 2012, 2014, 2016, 2018, and 2020 were selected. For spatial resampling, one out of every two data rows in the latitudinal direction were selected. Then, the 13,562,481 data pairs after spatiotemporal sampling were randomly divided into 10 parts, and 2 parts from all 10 parts were firstly selected as training samples, and then 1 part of the data pairs from the remaining 8 parts were randomly selected as validation samples. All impact factors datasets were normalized prior to input into the PM_{2.5} and O₃ estimation MTL model of each region. The shared layer number for the PM_{2.5} and O₃ estimation MTL model was set to 100, while the task-specific tower layer number for PM_{2.5} and O₃ were set to 120, and 120, respectively. To improve the robustness of the model, 10 random trials were conducted for the MTL model, and the average result of these 10 trials was considered as the final MTL model result of each region. The flowchart of this work is shown in Figure 1, below.

3.2. MTL Modelling Accuracy Validation

After the PM_{2.5} and O₃ estimation MTL models of three regions were established, the prediction accuracy of these three models were evaluated. In this work, two commonly used statistical indicators, including R^2 and root-mean-squared error (RMSE), were calculated between spatial-temporal co-located observed PM_{2.5} and O₃, and the model estimated PM_{2.5} and O₃ to quantitatively evaluate the model accuracy and performance. These two statistical indicators can be described as the following equations:

$$R^2 = 1 - \frac{\sum_{i=1}^n (o_i - f_i)^2}{\sum_{i=1}^n (o_i - \bar{o})^2} \quad (2)$$

$$RMSE = \sqrt{\frac{1}{n} \sum_{i=1}^n (f_i - o_i)^2} \quad (3)$$

where o_i denotes observed PM_{2.5} or O₃, f_i represents the estimated PM_{2.5} or O₃, \bar{o} is arithmetic means of the observed PM_{2.5} or O₃ values, and n denotes the number of data pairs.

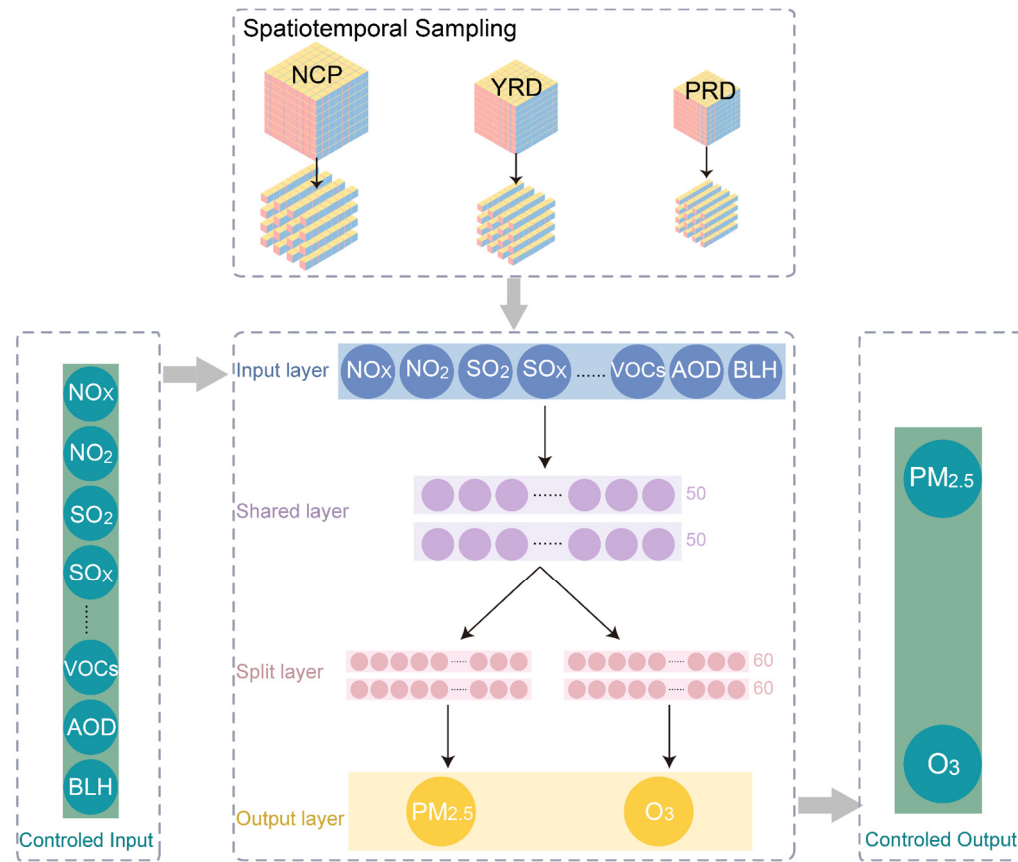


Figure 1. The flowchart of this work.

3.3. Relative Importance Evaluation and Estimation of the Impacts from Each Precursor

To evaluate the relative importance of each factor to the PM_{2.5} and O₃ collaborative pollution of each region, sensitivity analyses based on the PM_{2.5} and O₃ estimation MTL model are required to determine the contribution of each factor. Taking AOD as an example, a scenario without AOD was simulated by replacing the time series of AOD with zero, while all other factors remained unchanged (Equation (4)). Subsequently, the response of PM_{2.5} and O₃ to AOD (denoted as PM_{2.5-resp}, O_{3-resp} in Equation (5)) was modeled as the PM_{2.5} and O₃ difference between the original simulated PM_{2.5} and O₃ (denoted as Y_{PM_{2.5}}, Y_{O₃} in Equation (3)) and the later PM_{2.5} and O₃ simulated with the AOD time series was replaced with zero (denoted as Y'_{PM_{2.5}}, Y'_{O₃} in Equation (4)):

$$Y_{PM_{2.5}}, Y_{O_3} \sim MTL(NO_X, NO_2, SO_X, SO_2, AOD, BLH, VOCs, LULC1, LULC2, LULC3, LULC4, LULC5, LULC7, LULC8, LULC9, \text{Aerosol component}, NDVI, POPU, RH, SP, T, TCC, TP, UV, WD, WS, Month) \quad (4)$$

$$Y'_{PM_{2.5}}, Y'_{O_3} \sim MTL(NO_X, NO_2, SO_X, SO_2, AOD^*, BLH, VOCs, LULC1, LULC2, LULC3, LULC4, LULC5, LULC7, LULC8, LULC9, \text{Aerosol component}, NDVI, POPU, RH, SP, T, TCC, TP, UV, WD, WS, Month) \quad (5)$$

$$PM_{2.5-resp}, O_{3-resp} = Y_{PM_{2.5}}, Y_{O_3} - Y'_{PM_{2.5}}, Y'_{O_3} \quad (6)$$

where AOD* represents the masked AOD time series. PM_{2.5-resp} and O_{3-resp} denote the responses of PM_{2.5} and O₃ to AOD. Likewise, PM_{2.5} and O₃ responses to other influencing factors were also evaluated through such a sensitivity analysis scheme.

In addition, a similar method to the sensitivity analyses described above was also used to quantitatively estimate the impact of each precursor on PM_{2.5} and O₃. Taking NO_X as an example, a scenario of changes in NO_X concentration was modeled by replacing the

NO_x concentration in each day of 2011–2020 with NO_x values from the corresponding date in 2010, while all other factors remained unchanged. This scenario simulated a change in NO_x concentration using the NO_x concentration in 2010 as a baseline. Subsequently, the impact of NO_x on PM_{2.5} and O₃ (denoted as $PM_{2.5_resp}$, O_{3_resp} in Equation (8)) was calculated as the PM_{2.5} and O₃ difference between the simulated original PM_{2.5} and O₃ (denoted as $Y_{PM_{2.5}}$, Y_{O_3} in Equation (6)) and the PM_{2.5} and O₃ simulated with the NO_x time series replaced by NO_x concentration in each day of 2010 (denoted as $Y'_{PM_{2.5}}$, Y'_{O_3} in Equation (7)):

$$Y_{*PM_{2.5}}, Y_{*O_3} \sim MTL(NO_X, NO_2, SO_X, SO_2, VOCs, Aerosol component) \quad (7)$$

$$Y'_{PM_{2.5}}, Y'_{O_3} \sim MTL(NO_X^*, NO_2, SO_X, SO_2, VOCs, Aerosol component) \quad (8)$$

$$PM_{2.5_resp}^*, O_{3_resp}^* = Y_{*PM_{2.5}}, Y_{*O_3} - Y'_{PM_{2.5}}, Y'_{O_3} \quad (9)$$

where NO_X^* represents masked values of NO_X . $PM_{2.5_resp}^*$ and $O_{3_resp}^*$ denote the responses of PM_{2.5} and O₃ to NO_x. Likewise, PM_{2.5} and O₃ responses to other precursor factors were evaluated through this sensitivity analysis scheme. A brief introduction to the sensitivity analysis scheme can be found in the work of Ma et al. (2023) [17].

4. Results

4.1. Model Performance Verification

Figure 2 showed the sample-based validation results of these three MLT model-estimated PM_{2.5} and O₃ datasets in the NCP, the YRD, and the PRD. It indicated that MLT model-estimated PM_{2.5} and O₃ results exhibit a high correlation with the gridded surface PM_{2.5} and O₃ measurements in all three regions. The sample-based validation results in Figure 2 indicate that the prediction accuracy of these three models is high, the R² values of these three models were all larger than 0.69, and the RMSE values were all smaller than 16.95 $\mu\text{g m}^{-3}$. Among these three regions, the PM_{2.5} and O₃ estimation MLT model in the NCP had the highest predictive accuracy, with R² values of 0.79 and 0.82 for PM_{2.5} and O₃ estimation results, and RMSE values of 15.72 $\mu\text{g m}^{-3}$ and 16.15 $\mu\text{g m}^{-3}$ for PM_{2.5} and O₃ estimation results, respectively. In addition to the NCP, the accuracy of the PM_{2.5} and O₃ MLT estimation model for the YRD was the second highest among the models in these three regions, with R² values of 0.78 and 0.79, and RMSE values of 13.80 $\mu\text{g m}^{-3}$ and 16.02 $\mu\text{g m}^{-3}$ for PM_{2.5} and O₃ estimation results, respectively. Additionally, the accuracy of the PM_{2.5} and O₃ estimation MLT model in the PRD was also high, with R² values of 0.69 and 0.70, and RMSE values of 9.40 $\mu\text{g m}^{-3}$ and 16.95 $\mu\text{g m}^{-3}$ for PM_{2.5} and O₃ estimation results, respectively. In general, the PM_{2.5} and O₃ MLT estimation models in these three regions developed in this study can approximate the spatiotemporal variation patterns of O₃ and PM_{2.5} with high precision.

4.2. Relative Importance of Each Explanatory Variable

The relative importance of explanatory variables for surface PM_{2.5} and O₃ pollution in the NCP, the YRD, and the PRD are depicted in Figure 3. For PM_{2.5} and O₃ pollution in the NCP, the PRD, and the YRD, the PM_{2.5} and O₃ precursor-related variables (including HCHO, six kinds of VOC, aerosol component, SO₂, NO₂, SO_X, and NO_X) are the most critical of all influencing factors, with their relative importance ranging from 29.99% to 40.65%. Among these precursors, VOC (including HCHO, C₃H₈, C₅H₈, CH₄, H₂O₂, OH, and PAN) and aerosol components (including BCSM, DUSMASS25, and OCSM) are found to be the most important dominant precursors for both PM_{2.5} pollution and O₃ pollution in these three regions, with their relative importance values ranging from 22.66% to 33.17%. These results indicate that surface O₃ and PM_{2.5} pollution in these three regions are largely regulated by VOC, aerosol components, SO_X, and NO_X, which means that reducing the emissions of VOC, aerosols, SO_X, and NO_X can effectively reduce the O₃ and PM_{2.5} pollution levels in the NCP, the PRD, and the YRD.

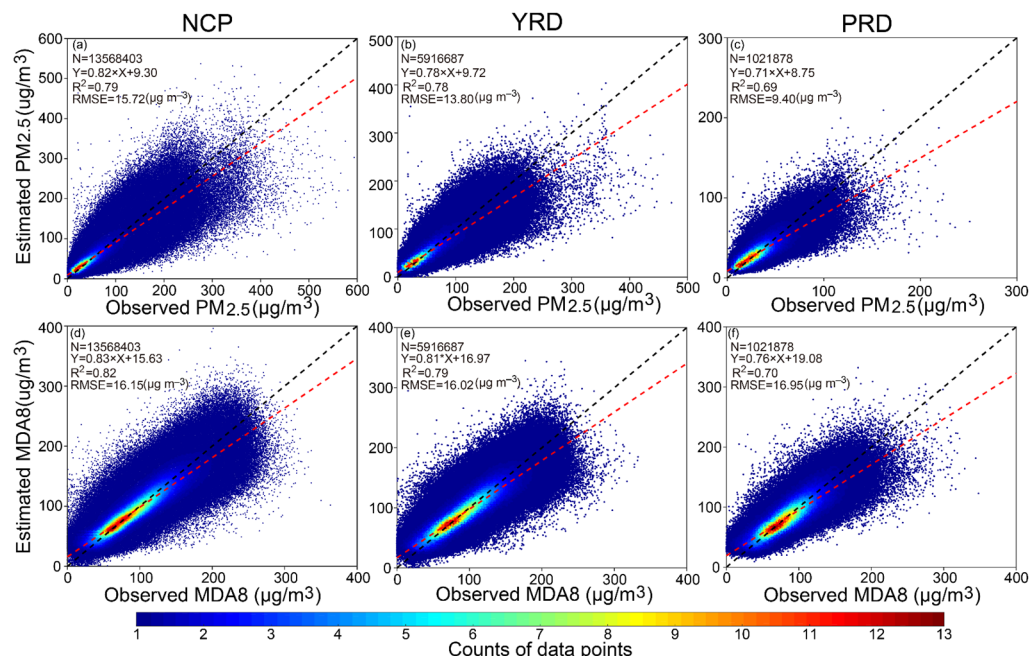


Figure 2. Density scatterplots of sample-based validation results of three PM_{2.5} and O₃ pollution estimation MTL models in the NCP, the YRD, and the PRD. Sample-based validation results of the surface PM_{2.5} and O₃ estimation results in the NCP are shown in (a,d), respectively, while (b,e) denote results for model-estimated surface PM_{2.5} and O₃ in the YRD. (c,f) indicate validation results of estimated surface PM_{2.5} and O₃ in the PRD.

In addition to precursor emission variables, meteorological factors are the second most important influencing variables on PM_{2.5} and O₃ pollution in the NCP, the YRD and the PRD, with the relative importance values of these meteorological factors ranging from 15.89% to 20.11%. These meteorological factors include surface UV radiation, surface 2 m temperature, relative humidity at 1000 hPa, boundary layer height, wind speed, wind direction, surface pressure, total precipitation, and total cloud cover. Among these meteorological variables, temperature, UV radiation, and relative humidity are the three most important meteorological factors for PM_{2.5} and O₃ pollution in the NCP, the YRD, and the PRD, with their relative importance values ranging from 1.84% to 3.99%. These results are consistent with previous studies [46–53], and high temperatures, strong UV radiation, and suitable relative humidity provide an appropriate environment to promote ozone photochemistry and the formation of ozone pollution. Similar to O₃ pollution, appropriate temperature and solar radiation, as well as high relative humidity also provide a suitable environment for the generation and concentration of PM_{2.5} pollution, which is also consistent with the results of previous studies [47,54–57]. Besides precursors and meteorological factors, there are several factors such as AOD, land use and land cover, NDVI, population, topography, and month that have a strong influence on PM_{2.5} and O₃ pollution in the NCP, the YRD, and the PRD, and their relative importance ranges from 21.40% to 23.46%. Among these variables, LULC2 and month are revealed to be the most important influencing factors for O₃ pollution in these three regions, with the relative importance larger than 1.74%, and 1.77%, respectively, while AOD and LULC2 are revealed to be the most important influencing factors for PM_{2.5} pollution in these three regions, with the relative importance larger than 1.74% and 3.84%, respectively.

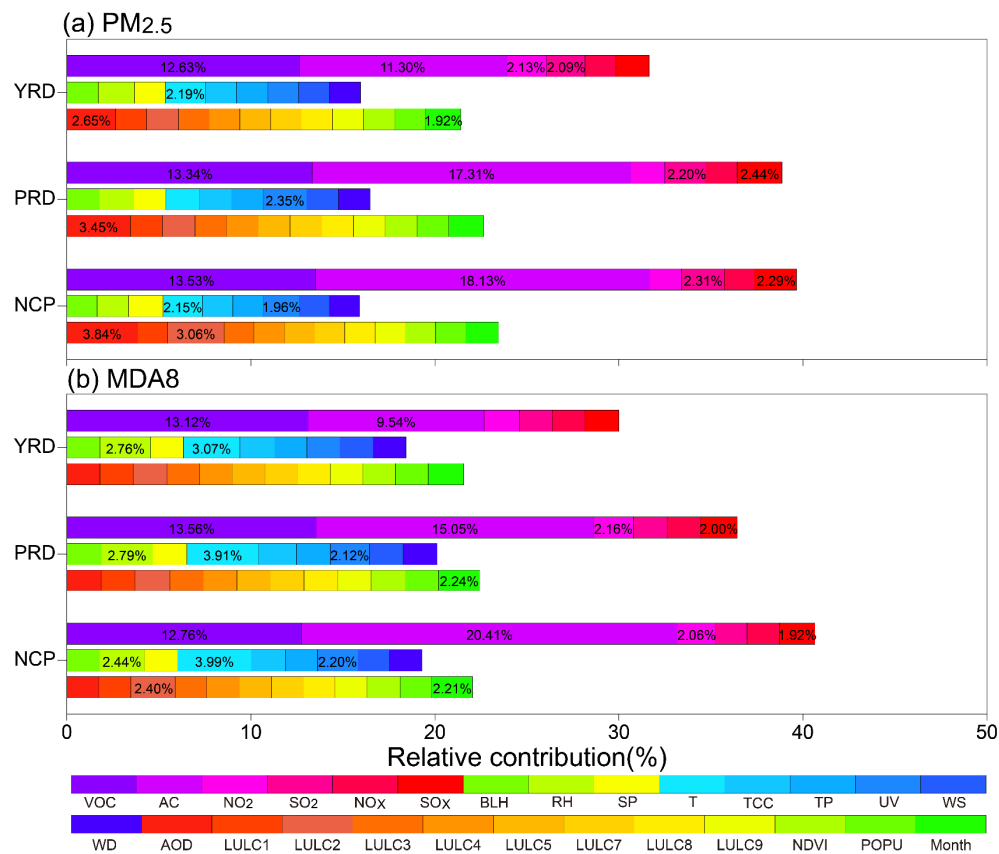


Figure 3. The relative importance of each explanatory variable to PM_{2.5} pollution and O₃ pollution using the MTL estimation models in the NCP, the PRD, and the YRD. In this figure, VOC represent HCHO and six kinds of Volatile Organic Compounds, including Hydrogen peroxide, Isoprene, Peroxyacetyl nitrate, Hydroxyl radicals, Methane and Propane. Aerosol Components represent three kinds of a mainly primary aerosol composition, including Black Carbon Surface Mass, Dust Surface Mass Density of PM2.5, and Organic Carbon Surface Mass.

4.3. PM_{2.5} and O₃ Collaborative Pollution Response to Each Precursor

To quantitatively estimate the impact of each precursor on the PM_{2.5} and O₃ collaborative pollution of each region, sensitivity analyses based on the PM_{2.5} and O₃ estimation MTL models are applied to determine the contribution of each factor. Taking the concentration of each precursor in 2010 as a baseline, a scenario of changes in this precursor concentration was modeled by replacing the concentration of this precursor in each day of 2011–2020 with values from the corresponding date in 2010, while all other influencing factors of PM_{2.5} and O₃ collaborative pollution remained unchanged. Subsequently, the impact of this specific precursor on PM_{2.5} and O₃ was calculated as the PM_{2.5} and O₃ difference between the simulated original PM_{2.5} and O₃, and the PM_{2.5} and O₃ simulated with this special precursor time series were replaced by its concentration from the corresponding date in 2010.

Figure 4 depicted the temporal patterns of the annual response of PM_{2.5} and O₃ pollution to each precursor during 2011–2020 estimated by the MTL models in the NCP, the PRD, and the YRD. The results showed that among these seven PM_{2.5} precursor factors, four influencing factors with the largest PM_{2.5} pollution response in these three regions were SO₂, HCHO, NO₂, and SO_x, and a 10-year average value of PM_{2.5} response for these four factors were larger than 0.30 $\mu\text{g m}^{-3}$. The variations of these four precursors had the greatest impact on PM_{2.5} pollution in these three regions, which means that emission reduction in these four precursors is the most effective measure to mitigate PM_{2.5} pollution in the NCP, the PRD, and the YRD. However, the two most crucial precursors of PM_{2.5} are different across these three regions. The two most important influencing factors on PM_{2.5}

pollution in the NCP (YRD) are SO_2 and HCHO , with 10-year averaged $\text{PM}_{2.5}$ response values of $2.64 \mu\text{g m}^{-3}$ ($2.01 \mu\text{g m}^{-3}$), and $1.71 \mu\text{g m}^{-3}$ ($0.95 \mu\text{g m}^{-3}$), respectively. However, the two most important impact factors on $\text{PM}_{2.5}$ pollution in the PRD are SO_2 and NO_x , with 10-year averaged $\text{PM}_{2.5}$ response values of $1.24 \mu\text{g m}^{-3}$ and $0.88 \mu\text{g m}^{-3}$, respectively.

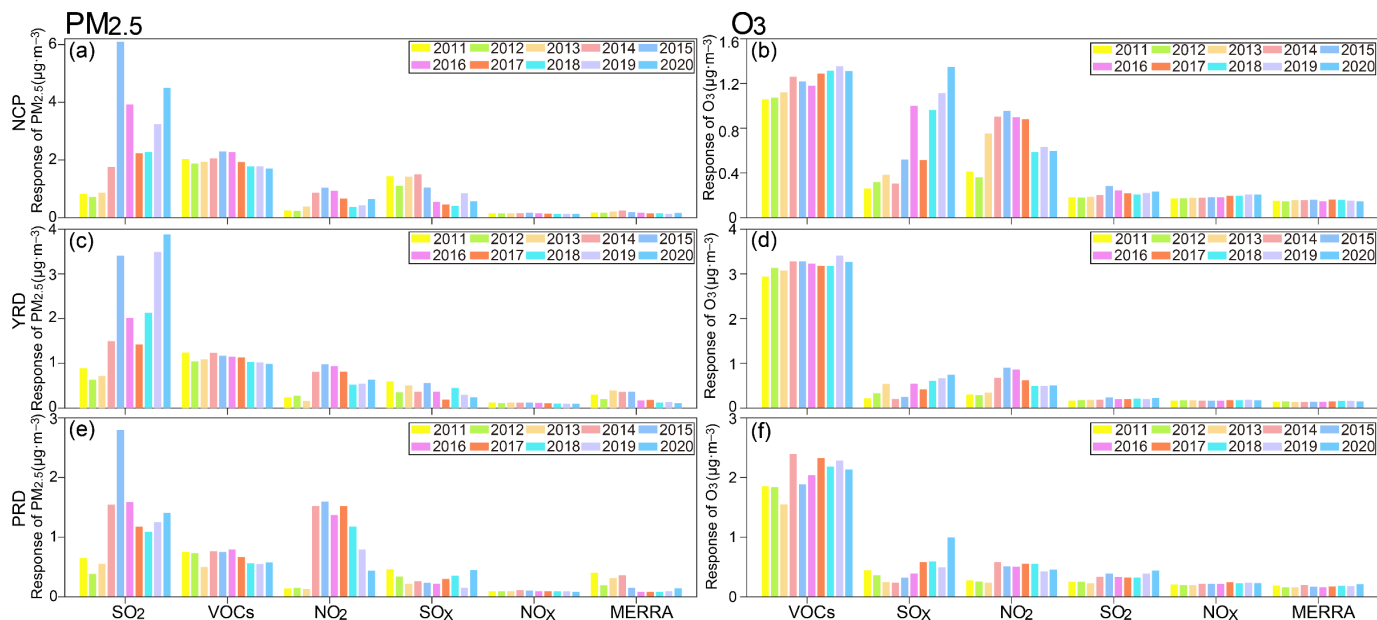


Figure 4. The annual response of $\text{PM}_{2.5}$ and O_3 pollution to each precursor in the NCP, the PRD, and the YRD during 2011–2020. The annual response of $\text{PM}_{2.5}$ pollution to each precursor in the NCP, the PRD, and the YRD are shown in (a,c,e), respectively, while (b,d,f) denote results for the annual response of O_3 pollution to each precursor in the NCP, the PRD, and the YRD.

In terms of O_3 pollution, it indicated that among these O_3 precursors, three influencing factors with the largest O_3 pollution response in these three regions were HCHO (the by-product of many VOC oxidation processes, and a critical proxy of VOC), NO_2 , and SO_x , and the 10-year average O_3 response values for these three factors were larger than $0.6 \mu\text{g m}^{-3}$. The variations of these three precursors had the greatest impact on O_3 pollution in these three regions, which means that the emission reduction in VOC, NO_2 , and SO_x is the most effective measure to mitigate O_3 pollution in the NCP, the PRD, and the YRD. Moreover, the two most crucial precursors of O_3 are different across these three regions. The two most important influencing factors on O_3 pollution in the NCP (YRD) are HCHO and NO_2 , with 10-year averaged O_3 response values of $1.00 \mu\text{g m}^{-3}$ ($2.89 \mu\text{g m}^{-3}$) and $0.70 \mu\text{g m}^{-3}$ ($0.55 \mu\text{g m}^{-3}$), respectively. However, the two most important impact factors on O_3 pollution in the PRD are HCHO and SO_x , with 10-year averaged O_3 response values of $1.79 \mu\text{g m}^{-3}$ and $0.47 \mu\text{g m}^{-3}$, respectively.

In terms of the temporal patterns of $\text{PM}_{2.5}$ and O_3 pollution responses to precursor variations, the responses of $\text{PM}_{2.5}$ and O_3 pollution to different precursor factors in different regions have different temporal variation features. For $\text{PM}_{2.5}$ pollution, the temporal variation patterns of the $\text{PM}_{2.5}$ pollution response to SO_2 in the NCP, the YRD, and the PRD were similar. And, the response values of $\text{PM}_{2.5}$ pollution to SO_2 in these three regions increased from 2011 to 2015, peaked in 2015, decreased from 2015 to 2017, reached a minimum value in 2017 (2018 for the PRD), then elevated again from 2017 (2018 for the PRD) to 2020, and reached a second peak in 2020. However, the temporal variation patterns of the response of $\text{PM}_{2.5}$ to HCHO in these three regions were different. The response values of $\text{PM}_{2.5}$ to HCHO in the NCP increased from 2011 to 2015, peaked in 2015, and decreased from 2015 to 2020, while the response values of $\text{PM}_{2.5}$ pollution to HCHO in the PRD and the YRD showed an overall decreasing trend from 2011 to 2020. The temporal variation patterns of the response values of $\text{PM}_{2.5}$ pollution to NO_2 in these three regions

were similar, and the response values of PM_{2.5} to NO₂ increased from 2011 to 2015, peaked in 2015, and then decreased from 2015 to 2020. In addition, the temporal variation patterns of the response values of PM_{2.5} pollution to SO_X in these three regions were different, and the response values of PM_{2.5} to SO_X in the NCP increased from 2011 to 2014, peaked in 2014, and then decreased from 2014 to 2020, while the response values of PM_{2.5} to SO_X in the PRD decreased from 2011 to 2016, reached a minimum value in 2016, and then increased from 2016 to 2020. Different from the response of PM_{2.5} to SO_X in the NCP and the PRD, the response values of PM_{2.5} to SO_X in the YRD showed an overall decreasing trend from 2011 to 2020. For O₃ pollution, the temporal variation patterns of the O₃ response to HCHO in the NCP, the YRD, and the PRD were similar. The response values of O₃ to HCHO in these three regions increased from 2011 to 2014, peaked in 2014, and decreased from 2014 to 2020. The temporal variation patterns of the response values of O₃ pollution to NO₂ in these three regions were similar, and the response values of O₃ to NO₂ increased from 2011 to 2015 (2014 for the PRD), peaked in 2015 (2014 for the PRD), and then decreased from 2015 (2014 for the PRD) to 2020. However, the temporal variation patterns of the response of O₃ to SO_X in these three regions were different. The response values of O₃ to SO_X in the NCP and the YRD showed an overall increasing trend from 2011 to 2020, while the response values of O₃ pollution to SO_X in the PRD decreased from 2011 to 2014, reached a minimum value in 2014, and then increased from 2014 to 2020. In addition, the temporal variation patterns of the response values of O₃ pollution to SO₂ in these three regions were different, and the response values of O₃ to SO₂ in the NCP and the YRD increased from 2011 to 2014, peaked in 2014, and then decreased from 2014 to 2020, while the response values of O₃ to SO₂ in the PRD increased from 2011 to 2015, reached a minimum value in 2015, decreased from 2015 to 2017, reached a minimum value in 2017, and then increased from 2017 to 2020. Different from the response of O₃ to HCHO, SO_X, NO₂, and SO₂ in these three regions, the response values of O₃ to VOC showed an overall increasing trend from 2011 to 2020.

Figure 5 depict the spatial patterns of the annual response of PM_{2.5} pollution to each precursor during 2011–2020 estimated by the MTL models in the NCP. The results indicated that among these precursors, SO₂, HCHO, SO_X, and NO₂ were the four most important precursors for PM_{2.5} pollution in the NCP, which was consistent with the results presented in Figure 4a. Among these precursors, the amplitude of PM_{2.5} response to SO₂ was the largest, with the values of the PM_{2.5} response to SO₂ higher than +12 $\mu\text{g m}^{-3}$ in parts of Shandong Province in 2015 and the PM_{2.5} response to SO₂ lower than −18 $\mu\text{g m}^{-3}$ in parts of the Jing-Jin-Ji (Beijing, Tianjin, and Hebei provinces) region in 2020. This may be related to the isotropic feedback of PM_{2.5} pollution on SO₂ [58]. Compared with 2010, the SO₂ concentration in (shown in Figure S1) 2011 in the NCP was relatively higher, so the response value of PM_{2.5} to SO₂ in 2011 was positive. From 2012 to 2013, SO₂ concentrations in the NCP were lower than those in 2010, especially in the Jing-Jin-Ji region (Beijing, Tianjin, and Hebei provinces) and the Lu-Yu region (Shandong and Henan provinces), so the response values of PM_{2.5} pollution to SO₂ were negative from 2012 to 2013. During 2014–2017, SO₂ concentrations in the NCP increased significantly and were larger than those in 2010, especially in Hebei, Shandong, Henan, and Shanxi provinces, so the response values of PM_{2.5} to SO₂ in 2014–2017 were positive, and the response value was largest in 2015. In contrast, SO₂ concentrations from 2014 to 2017 in Beijing and Tianjin were lower than those in 2010, so the response values of PM_{2.5} to SO₂ in Beijing and Tianjin were negative, and the response value was largest in 2017. From 2018 to 2020, SO₂ concentrations in the NCP were smaller than those in 2010, especially in the Jing-Jin-Ji region and the Lu-Yu region, so the response value of PM_{2.5} to SO₂ in 2018–2020 was negative, and the amplitude of the response value was largest in 2020.

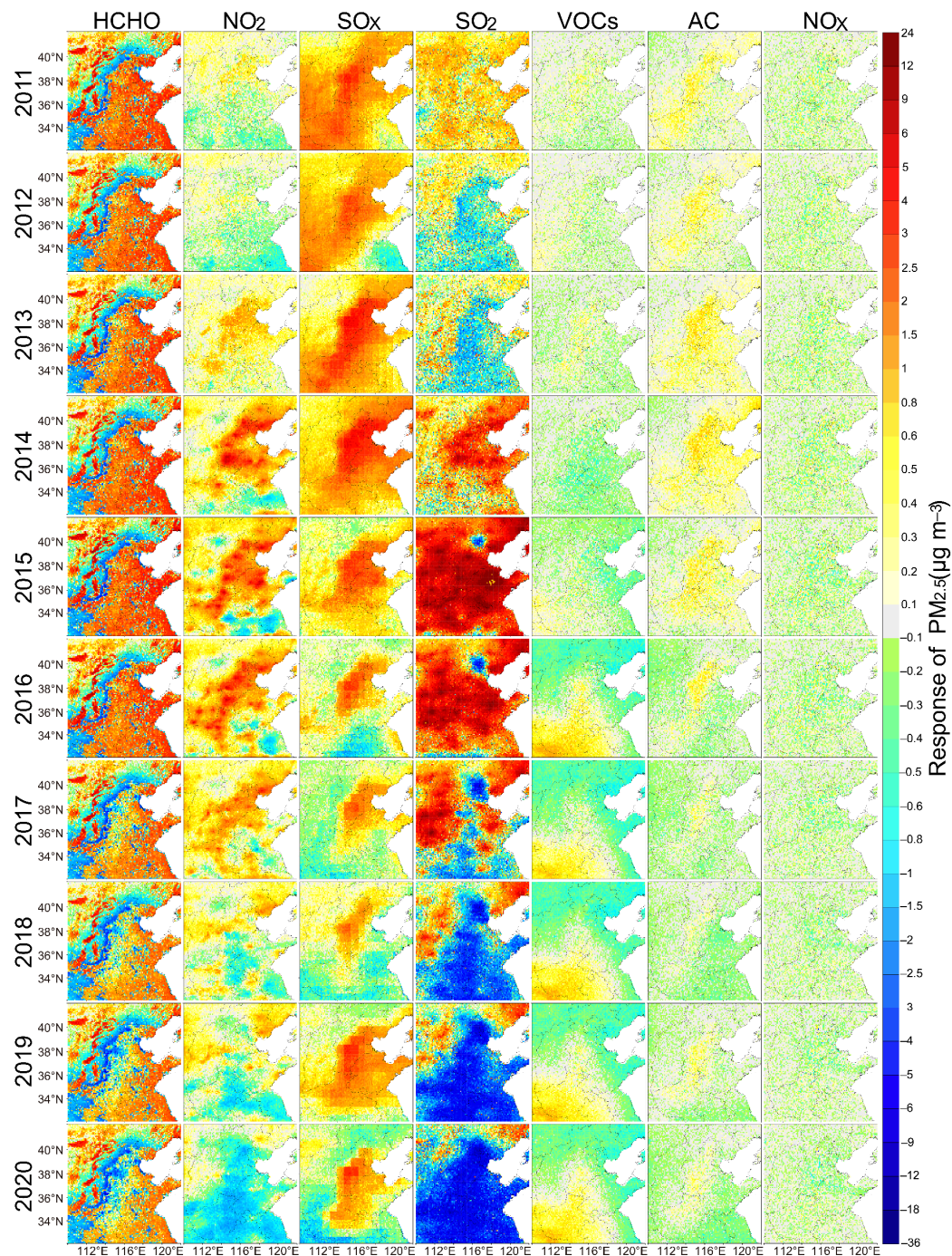


Figure 5. The spatial distribution of the annual response of PM_{2.5} pollution to each precursor in the NCP during 2011–2020.

In addition to SO₂, the amplitude of the response of PM_{2.5} pollution to HCHO (the by-product of many VOC oxidation processes, and a critical proxy of VOC) was the second largest among all precursors, with the PM_{2.5} response values to HCHO higher than $+6 \mu\text{g m}^{-3}$ in parts of the Ji-Lu-Yu (Hebei, Henan, and Shandong provinces) region in 2011. This may be related to the positive feedback of PM_{2.5} pollution on HCHO (also known as VOC). Compared with 2010, the HCHO (i.e., VOC) concentration in 2011–2020 in the main region of Ji-Lu-Yu was relatively higher, so the response value of PM_{2.5} to VOC in 2011–2020 was positive. However, the response value of PM_{2.5} to VOC in the main regions of the NCP increased during 2011–2015, reached the peak value in 2015, and then decreased during 2015–2020. Meanwhile, HCHO concentrations (shown in Figure S2) and the anthropogenic

emissions of VOC (shown in Figure S3) showed an overall increasing trend from 2010 to 2020. This may be related to the nonlinear relationship between HCHO (VOC emissions) and PM_{2.5} pollution in the NCP [57,59–61]. Before 2015, VOC emissions were not saturated for PM_{2.5} pollution, and the positive response of PM_{2.5} pollution increased gradually with the increase in VOC emissions. However, VOC emissions began to saturate for PM_{2.5} pollution after 2015, and the contribution of rising VOC emissions to the increase in PM_{2.5} pollution levels is gradually declining, where the positive response of PM_{2.5} pollution gradually decreased with the increase in VOC emissions between 2015 and 2020.

Besides SO₂ and HCHO, the amplitude of the response of PM_{2.5} pollution to SO_X is the third largest among all precursors, with the PM_{2.5} response values to SO_X higher than +4 $\mu\text{g m}^{-3}$ in parts of the Ji-Lu-Yu region in 2014. This may be due to the positive feedback of PM_{2.5} pollution on SO_X. Compared with 2010, the SO_X concentration (shown in Figure S4) in 2011–2020 in the main region of Ji-Lu-Yu was relatively higher, so the response value of PM_{2.5} to SO_X in 2011–2020 was positive. However, the response value of PM_{2.5} to SO_X in the main regions of the NCP increased during 2011–2014, reached the peak value in 2014, and then decreased during 2014–2020. Meanwhile, SO_X concentrations (shown in Figure S6) increased from 2010 to 2014, and then decreased during 2014–2020.

Moreover, the amplitude of the response of PM_{2.5} pollution to NO₂ is the fourth largest among all precursors, with PM_{2.5} response values to NO₂ higher than +3 $\mu\text{g m}^{-3}$ in parts of the Ji-Lu-Yu region in 2015. This may be due to the positive feedback of PM_{2.5} pollution on NO₂ [33,62,63]. Compared with 2010, the NO₂ concentration (shown in Figure S5) in 2011–2012 in the central and southern NCP was lower, so the response value of PM_{2.5} to NO₂ in 2011–2012 was negative. However, the NO₂ concentration in 2013–2017 in the main part of the NCP was relatively higher, so the response value of PM_{2.5} to NO₂ in 2013–2017 was positive. From 2018 to 2020, the NO₂ concentration in the main part of the NCP was relatively lower, so the response value of PM_{2.5} to NO₂ in 2018–2020 was negative. Compared with these four precursors, the response of PM_{2.5} pollution to CAMS-VOC, aerosol component, and NO_X were relatively smaller.

Figure 6 depicts the spatial patterns of the annual response of O₃ pollution to each precursor during 2011–2020 estimated by the MTL models in the NCP. The results indicated that among these precursors, HCHO, NO₂, SO_X, and VOC were the most important four precursors for O₃ pollution in the NCP, which was consistent with the results shown in Figure 4b. Among these precursors, the amplitude of the O₃ response to HCHO was the largest, with O₃ response values to HCHO higher than +5 $\mu\text{g m}^{-3}$ in northwestern parts of the NCP. This may be due to the different response patterns of O₃ to HCHO in different regions. In the Ji-Lu-Yu region, the response of O₃ pollution to HCHO was negative, and the level of O₃ pollution decreased with the increase in HCHO concentration. Compared with 2010, the HCHO concentration (shown in Figure S2) in 2011–2020 in the Ji-Lu-Yu region was relatively higher, so the response value of O₃ to HCHO was negative during 2011–2020. In contrast, the responses of O₃ pollution to HCHO in the northwestern part of the NCP (Shanxi province and northwest part of Hebei province) and southeastern part of the NCP (Anhui province, the Jiangsu province, and the southeast part of Shandong province) were negative from 2011 to 2016, and then turned positive from 2017 to 2020. The level of O₃ pollution in the northwestern and northwest parts of the NCP increased with the decrease in HCHO concentration between 2011 and 2016, and then increased with the increase in HCHO concentration between 2017 and 2020. Compared with 2010, the HCHO concentration in 2011–2016 in the northwestern and northwest parts of the NCP was relatively lower, and the response value of O₃ to HCHO in this region was positive during 2011–2016; however, the HCHO concentration in 2017–2020 in this region was relatively higher, and the response value of O₃ to HCHO in this region was positive during 2017–2020.

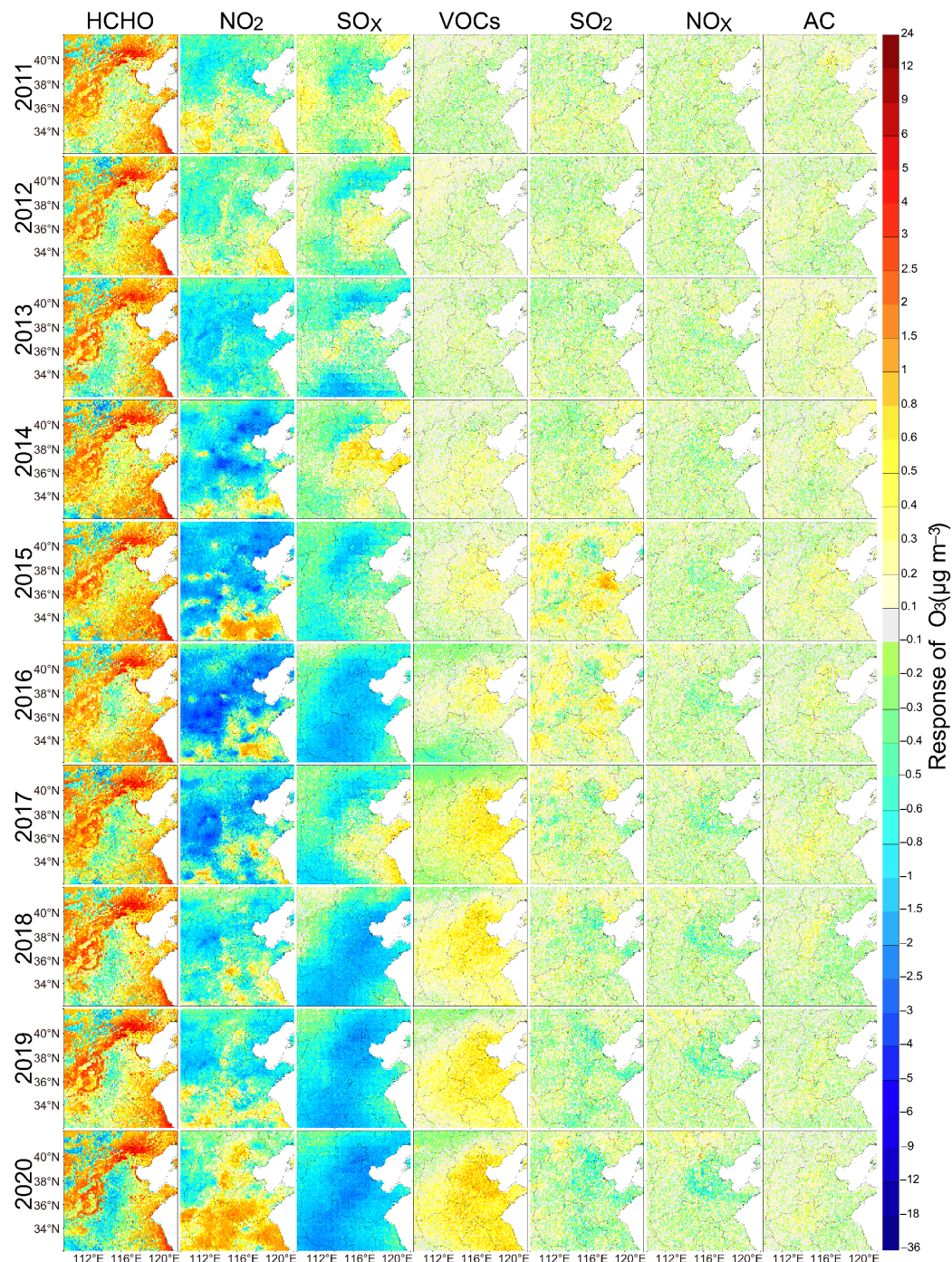


Figure 6. The spatial distribution of the annual response of O₃ pollution to each precursor in the NCP during 2011–2020.

For NO₂, the response value of O₃ pollution to NO₂ in the main region of the NCP decreased from 2011 to 2016, reached a minimum value in 2016, and then increased from 2016 to 2020. This may be related to the negative feedback of O₃ pollution on NO₂ [64,65]. The NO₂ concentration in 2011–2012 in the main region of the NCP was relatively lower than that in 2010, and the response value of O₃ to NO₂ in 2011–2012 was positive. Compared with 2010, NO₂ concentration (shown in Figure S5) in the NCP increased from 2013 to 2016 and was relatively higher, and the response value of O₃ pollution to NO₂ was negative and decreased from 2013 to 2016. Compared to 2010, NO₂ concentrations in the NCP were relatively higher between 2017 and 2019 and relatively lower in 2020, and NO₂ concentrations decreased from 2017 to 2020. Meanwhile, the response value of O₃ pollution

to NO_2 decreased from 2017 to 2020, and the response value was negative between 2017 and 2019 and was positive in 2020.

During 2011–2020, the response value of O_3 pollution to SO_X in the NCP increased between 2011 and 2014, reached the peak value in 2014, and then decreased from 2014 to 2020. This may be related to the isotropic feedback of O_3 pollution on SO_X . The SO_X emission in the northern Hebei province, Beijing, and Tianjin in 2011–2015 were smaller than that in 2010 (shown in Figure S4), so the response value of O_3 to SO_X was negative in this region from 2011 to 2015, while the SO_X in the border area of the Hebei, Henan, and Shandong provinces in 2011–2015 were larger than that in 2010, so the response value of O_3 to SO_X was positive in this region during 2011–2015. Meanwhile, SO_X emission in the NCP during 2016–2020 was lower than that in 2010; therefore, the response value of O_3 to SO_X in 2016–2020 is negative in the NCP.

For VOC, the response of O_3 to VOC in the NCP increased from $0.1 \mu\text{g m}^{-3}$ in 2011 to $2 \mu\text{g m}^{-3}$ in 2020. This may be related to the isotropic feedback of O_3 pollution on VOC in the NCP [66–68]. VOC emissions in the NCP increased from 2011 to 2020 and were relatively higher than that in 2010 (shown in Figure S3), and the response value of O_3 pollution to VOC was positive and increased from 2011 to 2020. Compared with these four precursors, the response of O_3 pollution to SO_2 , NO_X , and aerosol components were relatively smaller.

Figure 7 depicts the spatial patterns of the annual response of $\text{PM}_{2.5}$ pollution to each precursor during 2011–2020 estimated by the MTL models in the YRD. Similar with the NCP, the results indicated that among these precursors, SO_2 , HCHO, NO_2 , and SO_X were the four most important precursors for $\text{PM}_{2.5}$ pollution in the YRD, which was consistent with the results presented in Figure 4c. Among all precursors, the amplitude of the $\text{PM}_{2.5}$ response to SO_2 was the largest, with the values of the $\text{PM}_{2.5}$ response to SO_2 higher than $+9 \mu\text{g m}^{-3}$ in the south part of Jiangsu province in 2015 and the $\text{PM}_{2.5}$ response to SO_2 lower than $-12 \mu\text{g m}^{-3}$ in the north parts of the YRD in 2020. This may be due to the isotropic feedback on $\text{PM}_{2.5}$ pollution to SO_2 . Compared with 2010, the SO_2 concentration (shown in Figure S6) in 2011 in the YRD was relatively high, so the response value of $\text{PM}_{2.5}$ to SO_2 in 2011 was positive. From 2012 to 2013, the SO_2 concentration in the YRD was lower than that in 2010, especially in the north part of the YRD, so the response values of $\text{PM}_{2.5}$ pollution to SO_2 were negative from 2012 to 2013. However, the SO_2 concentration in the YRD increased significantly in 2014–2017, and was larger than that in 2010, so the response values of $\text{PM}_{2.5}$ to SO_2 in 2014–2017 were positive. Meanwhile, the amplitude of the response value increased between 2014 and 2015, reached the peak value in 2015, and then decreased in 2016–2017. From 2018 to 2020, the SO_2 concentration in the YRD decreased significantly and was lower than that in 2010, especially in the north part of the YRD, so the response value of $\text{PM}_{2.5}$ to SO_2 in 2018–2020 was negative, and the response value decreased in 2018–2020.

In addition to SO_2 , the amplitude of the response of $\text{PM}_{2.5}$ pollution to HCHO is the second largest among all precursors, with the $\text{PM}_{2.5}$ response values to HCHO higher than $+2.5 \mu\text{g m}^{-3}$ in the north parts of the YRD in 2011. This may be due to the different response patterns of $\text{PM}_{2.5}$ pollution to HCHO in different regions. The response of $\text{PM}_{2.5}$ to HCHO in the southern part of the YRD (including the southern part of the Anhui province, the northern part of Zhejiang province, and Shanghai) were likely due to negative feedback between 2011 and 2020. HCHO concentration (shown in Figure S7) in the southern part of the YRD increased in 2011–2020, and was higher than that in 2010, but the responses of $\text{PM}_{2.5}$ to HCHO were negative during 2011–2020 in this region. In the scenarios simulated by the MTL model, simulated $\text{PM}_{2.5}$ concentration decreased in 2011–2020 when it was compared with that in 2010. However, the response of $\text{PM}_{2.5}$ to HCHO in the northern part of the YRD (including the northern part of the Anhui province and the Jiangsu province) were likely due to negative feedback between 2011 and 2015 and turned to be positive feedback between 2016 and 2020. The HCHO concentration in the northern part of the YRD decreased in 2011–2015, and was lower than that in 2010, and the responses of $\text{PM}_{2.5}$

to HCHO were positive during 2011–2015 in this region, while HCHO concentration in this region increased in 2016–2020, and was higher than that in 2010, and the responses of PM_{2.5} to HCHO were positive during 2016–2020 in this region.

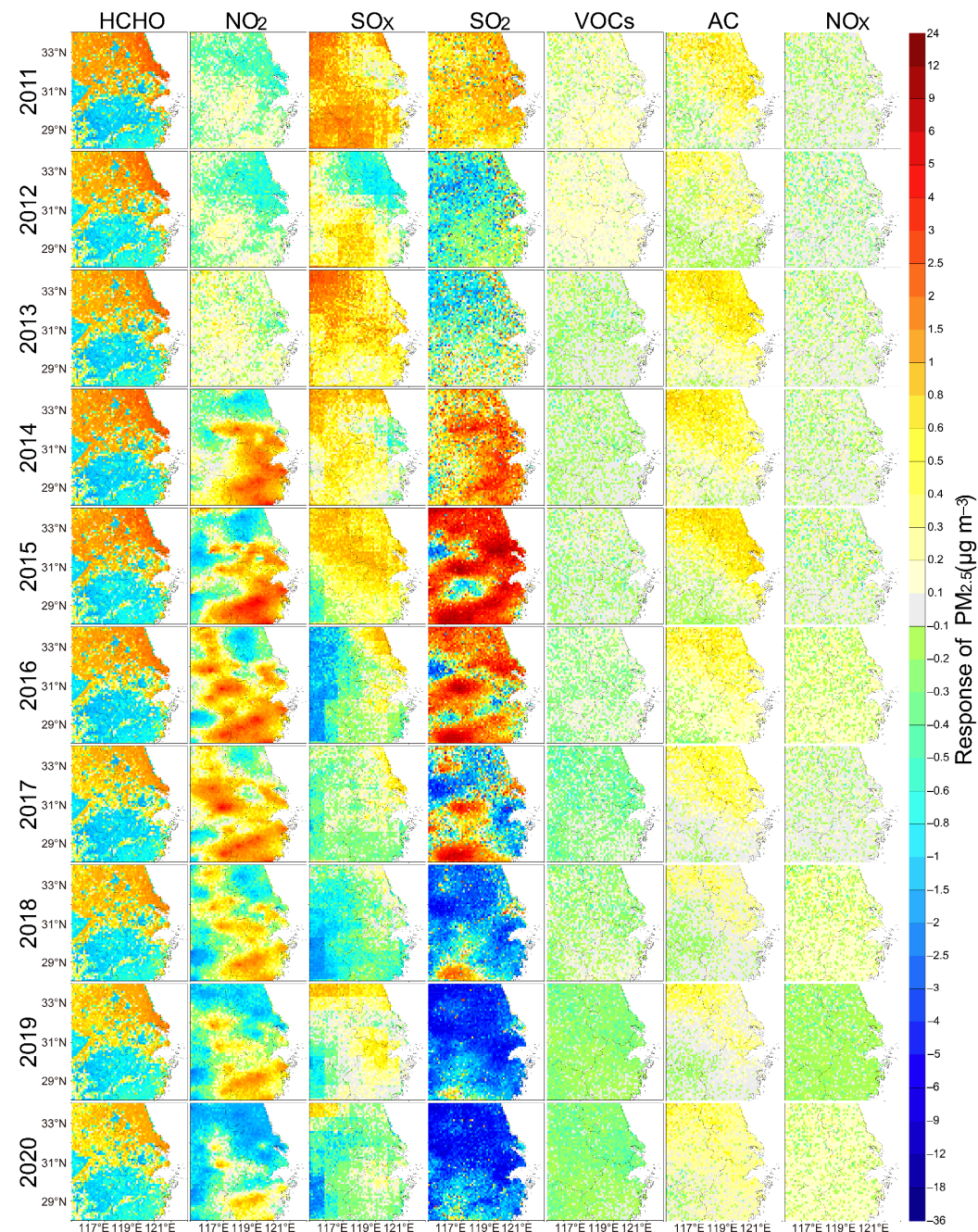


Figure 7. The annual spatial distribution of the response of PM_{2.5} pollution to each precursor in the YRD during 2011–2020.

Besides SO₂ and HCHO, the amplitude of the response of PM_{2.5} pollution to NO₂ is the third largest among all precursors, with PM_{2.5} response values to NO₂ higher than +5 $\mu\text{g m}^{-3}$ in the central and southern YRD in 2015. This may be due to the positive feedback of PM_{2.5} pollution on NO₂ [33,62,63]. Compared with 2010, the NO₂ concentration (shown in Figure S8) in 2011–2012 in the northeastern part of the YRD was lower, so the response value of PM_{2.5} to NO₂ in 2011–2012 was negative in this region, while the NO₂ concentration in 2011–2012 in the central part of the YRD was higher, so the response value of PM_{2.5} to NO₂ in 2011–2012 was positive in this region. Moreover, the NO₂ concentration in 2013

in the YRD was relatively higher than that in 2010, so the response value of PM_{2.5} to NO₂ in 2013 was positive. From 2014 to 2020, the NO₂ concentration in the northern YRD was relatively lower than that in 2010, so the response value of PM_{2.5} to NO₂ in 2014–2020 was negative in this region, while NO₂ concentration in the central and southern YRD was relatively higher than that in 2010, so the response value of PM_{2.5} to NO₂ in the central and southern YRD was positive from 2014 to 2020.

Moreover, the amplitude of the response of PM_{2.5} pollution to SO_X is the fourth largest among all precursors, with PM_{2.5} response values to SO_X higher than +3 $\mu\text{g m}^{-3}$ in the Anhui province in 2013. This may be due to the positive feedback of PM_{2.5} pollution to SO_X. SO_X concentrations in 2011, 2013–2015, and 2019 in the YRD were relatively higher than that in 2010 (shown in Figure S9), so the response values of PM_{2.5} to SO_X in 2011, 2013–2015, and 2019 were positive. However, SO_X concentrations in 2012 in the northern YRD were relatively lower than that in 2010, so the response values of PM_{2.5} to SO_X in 2012 were negative in northern YRD, while SO_X concentrations in 2012 in southern YRD were relatively higher than that in 2010, so the response values of PM_{2.5} to SO_X in 2012 were positive in the southern YRD. In addition, SO_X concentrations in 2016–2018 and 2020 in the YRD were relatively lower than that in 2010, so the response values of PM_{2.5} to SO_X in 2016–2018 and 2020 were negative in the YRD. Compared with these four precursors, the response of PM_{2.5} pollution to CAMS-VOC, aerosol components, and NO_X were relatively smaller.

Figure 8 depicts the spatial patterns of the annual response of O₃ pollution to each precursor during 2011–2020 estimated by the MTL models in the YRD. It indicated that among these precursors, HCHO, NO₂, SO_X, and VOC were the most important four precursors for O₃ pollution in the YRD, which is consistent with the results presented in Figure 4d. Among these precursors, the amplitude of the O₃ response to HCHO was the largest in 2015, with the O₃ response to HCHO higher than +9 $\mu\text{g m}^{-3}$ in eastern parts of the Jiangsu province. This may be due to the different response patterns of O₃ to HCHO in different regions. The response of O₃ to HCHO in the southern part of the YRD (including the southern part of the Anhui province, the northern part of the Zhejiang province, and Shanghai) were likely due to negative feedback between 2011 and 2020. HCHO concentration (shown in Figure S7) in the southern part of the YRD increased in 2011–2020, and was higher than that in 2010, but the responses of O₃ to HCHO were negative during 2011–2020 in this region. However, the response of O₃ to HCHO in the northern part of the YRD (including the northern part of the Anhui province and the Jiangsu province) were likely due to negative feedback between 2011 and 2015, and turned to be positive feedback between 2016 and 2020. HCHO concentration in the northern part of the YRD decreased in 2011–2015, and was lower than that in 2010, and the responses of O₃ to HCHO were positive during 2011–2015 in this region, while HCHO concentration in this region increased in 2016–2020 and was higher than that in 2010, and the responses of O₃ to HCHO were positive during 2016–2020 in this region.

For NO₂, the response value of O₃ pollution to NO₂ in the main region of the YRD decreased from 2011 to 2016, reached a minimum value in 2016, and then increased from 2016 to 2020. This may be related to the negative feedback of O₃ pollution on NO₂ [64,65]. The NO₂ concentration (shown in Figure S8) in 2011–2012 in northeastern YRD was relatively lower than that in 2010, and the response value of O₃ to NO₂ in 2011–2012 was positive, while NO₂ concentration in 2011–2012 in the central part of the YRD was higher, so the response value of O₃ to NO₂ in 2011–2012 was negative in this region. Moreover, the NO₂ concentration in 2013 in the main part of the YRD was relatively higher than that in 2010, so the response value of O₃ to NO₂ in 2013 was negative. From 2014 to 2020, the NO₂ concentration in northern YRD was relatively lower than that in 2010, and the response value of O₃ to NO₂ in 2014–2020 was positive in this region, while the NO₂ concentration in central and southern YRD were relatively higher than that in 2010, and the response value of O₃ to NO₂ in central and southern YRD were negative from 2014 to 2020.

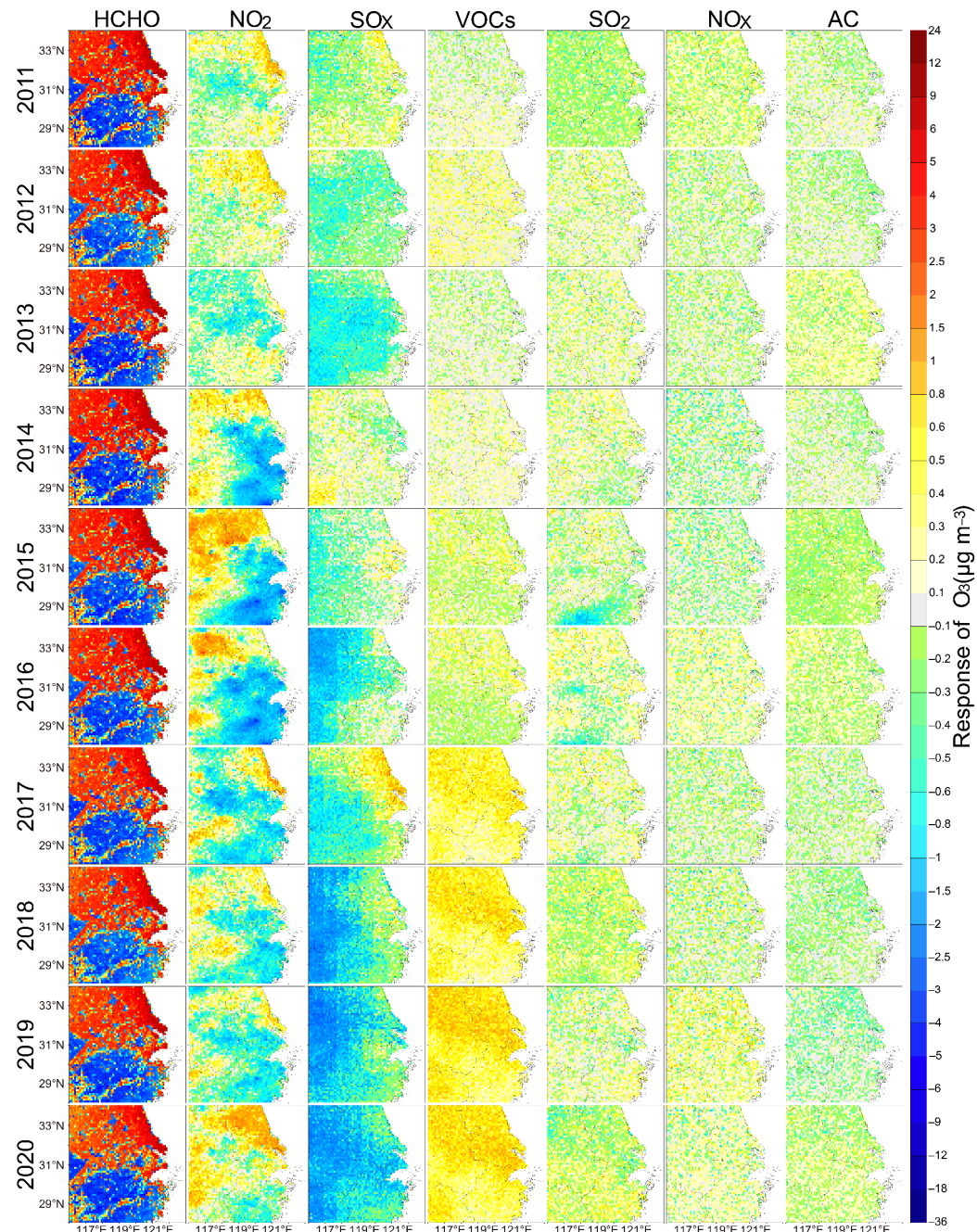


Figure 8. The annual spatial distribution of the response of O_3 pollution to each precursor in the YRD during 2011–2020.

Moreover, the amplitude of the response of O_3 pollution to SO_x is the third largest among all precursors, with O_3 response values to SO_x lower than $-3 \mu\text{g m}^{-3}$ in the Anhui province in 2020. This may be due to the different response patterns of O_3 pollution to SO_x in different regions. The responses of O_3 to SO_x in the YRD were likely due to negative feedback in 2011. From 2012 to 2013, the responses of O_3 to SO_x in the Jiangsu province were likely due to positive feedback, while the responses of O_3 to SO_x in the Anhui and Zhejiang provinces were likely due to negative feedback. In addition, from 2014 to 2020, the responses of O_3 to SO_x in the YRD were likely due to positive feedback. In 2011, SO_x concentrations in the southwestern region of the YRD were relatively higher than that in 2010 (shown in Figure S9), so the response values of O_3 to SO_x in 2011 were negative, while SO_x concentrations in the northeastern region of the YRD were relatively lower than that

in 2010, and the response values of O_3 to SO_X in this region were positive. However, from 2012 to 2013, SO_X concentrations in the northeastern region of the YRD were relatively lower than that in 2010, so the response values of O_3 to SO_X in this region were negative, while SO_X concentrations in the other parts of the YRD were relatively higher than that in 2010, and the response values of O_3 to SO_X in these regions were negative. In addition, during 2014–2020, SO_X concentrations in the main part of the YRD were relatively lower than that in 2010, so the response values of O_3 to SO_X were negative in this region; however, SO_X concentrations in western YRD in 2014, and in Shanghai and the Jiangsu province in 2017, were higher than those in 2010, and, therefore, the values of the O_3 response to SO_X were positive in these regions.

For VOC, the response of O_3 to VOC in the YRD increased from $0.1 \mu g m^{-3}$ in 2011 to $1.5 \mu g m^{-3}$ in 2020. This may be related to the isotropic feedback of O_3 pollution on VOC in the YRD [66–68]. VOC emissions in the YRD increased from 2011 to 2020 and were relatively higher than that in 2010 (shown in Figure S10), and the response value of O_3 pollution to VOC was positive and increased from 2011 to 2020. Compared with these four precursors, the response of O_3 pollution to SO_2 , NO_X , and aerosol components were relatively smaller.

Figure 9 depicts the spatial patterns of the annual response of $PM_{2.5}$ pollution to each precursor during 2011–2020 estimated by the MTL models in the PRD. Similar with the NCP and the YRD, the results indicated that among these precursors, SO_2 , NO_2 , HCHO, and SO_X were the four most important precursors for $PM_{2.5}$ pollution in the PRD, which are consistent with the results present in Figure 4e. Among these precursors, the amplitude of the $PM_{2.5}$ response to SO_2 was the largest, with the values of the $PM_{2.5}$ response to SO_2 higher than $+6 \mu g m^{-3}$ in the western region of the PRD in 2015 and the $PM_{2.5}$ response to SO_2 lower than $-12 \mu g m^{-3}$ in the central part of the PRD in 2020. This may be due to the isotropic feedback of $PM_{2.5}$ pollution on SO_2 [58]. Compared with 2010, SO_2 concentration (shown in Figure S11) in 2011, and 2013–2014, in the PRD was relatively higher, so the response value of $PM_{2.5}$ to SO_2 in 2011, and 2013–2014, were positive. In 2012, SO_2 concentration in the PRD was lower than that in 2010, and the values of the $PM_{2.5}$ response to SO_2 were negative. In the northwestern part of the PRD, the SO_2 concentration was larger than that in 2010, but it decreased significantly from 2015 to 2020, and, therefore, values of the $PM_{2.5}$ response to SO_2 were all positive in 2015–2020, but the spatial extent covered by positive values gradually decreased. In contrast, the SO_2 concentration in the southeastern part of the PRD was lower than that in 2010, and it decreased significantly from 2015 to 2020, and, therefore, values of the $PM_{2.5}$ response to SO_2 were all negative in this period, but the spatial extent covered by negative values gradually increased.

In addition to SO_2 , the amplitude of the $PM_{2.5}$ response to NO_2 was the second largest among all precursors, with values of the $PM_{2.5}$ response to NO_2 higher than $+5 \mu g m^{-3}$ in western PRD in 2014. This may be due to the positive feedback of $PM_{2.5}$ pollution on NO_2 [33,62,63]. In 2011–2013, NO_2 concentration (shown in Figure S12) in the PRD was lower than that in 2010, so values of $PM_{2.5}$ response to NO_2 were negative in this region. From 2014 to 2020, the NO_2 concentration in the main part of the PRD was relatively higher than that in 2010, so value of the $PM_{2.5}$ response to NO_2 was positive. Moreover, NO_2 concentrations in the southeastern part of the PRD between 2015 and 2019 and in the southern part of the PRD in 2020 were relatively lower than that in 2010, so the response value of $PM_{2.5}$ to NO_2 was negative.

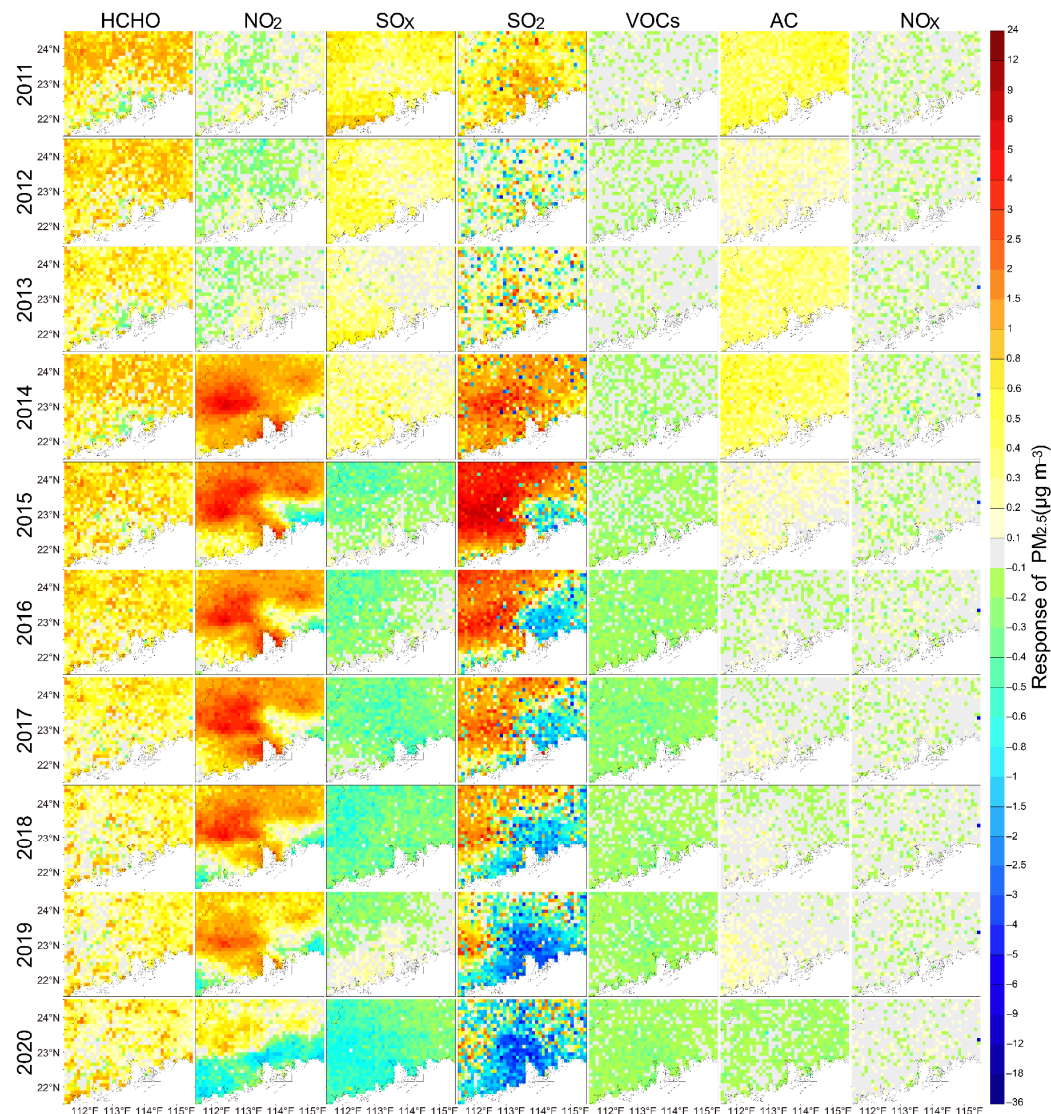


Figure 9. The annual spatial distribution of the response of $\text{PM}_{2.5}$ pollution to each precursor in the PRD during 2011–2020.

Besides SO_2 and NO_2 , the amplitude of the response of $\text{PM}_{2.5}$ pollution to HCHO is the second largest among all precursors, with the $\text{PM}_{2.5}$ response values to HCHO higher than $+2 \mu\text{g m}^{-3}$ in north parts of the PRD in 2011. This may be due to the different response patterns of $\text{PM}_{2.5}$ pollution to HCHO in different regions. The response of $\text{PM}_{2.5}$ to HCHO was likely due to negative feedback in northwestern PRD in 2011 and the entire PRD in 2013, while the response of $\text{PM}_{2.5}$ to HCHO was likely due to positive feedback in central and southeastern PRD in 2011, and in the entire PRD in 2012 and 2014–2020. The HCHO concentration (shown in Figure S13) was lower in the northwestern YRD in 2011, and the entire PRD in 2013, than that in 2010, and then values of the $\text{PM}_{2.5}$ response to HCHO were positive. Moreover, the HCHO concentration was higher in central and southeastern PRD in 2011, and in the entire PRD in 2012 and 2014–2020, than that in 2010, and then values of the $\text{PM}_{2.5}$ response to HCHO were positive. HCHO concentration increased between 2014 and 2020; however, the positive values of the $\text{PM}_{2.5}$ response to HCHO decreased in this period. This may be related to the nonlinear relationship between HCHO (VOC emissions) and $\text{PM}_{2.5}$ pollution in the PRD [57,59–61]. After 2014, HCHO (VOC emissions) began to saturate for $\text{PM}_{2.5}$ pollution, and the contribution of rising HCHO (VOC emissions) to the increase in $\text{PM}_{2.5}$ pollution levels gradually declined, and the positive response of $\text{PM}_{2.5}$ pollution gradually decreased with the increase in VOC emissions between 2015 and 2020.

Moreover, the amplitude of the response of PM_{2.5} pollution to SO_X is the fourth largest among all precursors, with the PM_{2.5} response values to SO_X higher than +1 $\mu\text{g m}^{-3}$ in the southwestern province in 2011. This may be due to the positive feedback of PM_{2.5} pollution on SO_X. SO_X concentrations decreased between 2011 and 2020 and were higher in 2011–2014 than that in 2010 (shown in Figure S14), so the response values of PM_{2.5} to SO_X in 2011–2014 were positive, while SO_X concentrations were lower in 2015–2020 than that in 2010, and, therefore, values of the PM_{2.5} response to SO_X in 2015–2020 were negative. Compared with these four precursors, the response of PM_{2.5} pollution to CAMS-VOC, aerosol components, and NO_X were relatively smaller.

Figure 10 depicts the spatial patterns of the annual response of O₃ pollution to each precursor during 2011–2020 estimated by the MTL models in the PRD. It indicated that among these precursors, HCHO, NO₂, SO_X, SO₂, and VOC were the most important five precursors for O₃ pollution in the PRD, which are consistent with the results present in Figure 4f. Among these precursors, the amplitude of the O₃ response to HCHO was the largest in 2015, with the values of the O₃ response to HCHO higher than +4 $\mu\text{g m}^{-3}$ in northern parts of the PRD. This may be due to the different response patterns of O₃ to HCHO in different regions. The response of O₃ to HCHO in central PRD was likely due to negative feedback in 2011–2012 and in 2014–2020, while the response of O₃ to HCHO in the other regions of the PRD, except the central part, was likely due to positive feedback in 2012 and in 2014–2020. Except for the central region of the PRD, the response of O₃ to HCHO was likely due to negative feedback in 2011, and in contrast, the response was likely due to positive feedback in 2013. The HCHO concentration was higher in central PRD in 2011–2012, and 2014–2020, than that in 2010, but the responses of O₃ to HCHO were negative, while the HCHO concentration was higher in the other regions of the PRD, except the central part, in 2012 and 2014–2020 than that in 2010, and then the responses of O₃ to HCHO were positive. The HCHO concentration was lower in 2011 in the other regions of the PRD, except the central part, than that in 2010, but the responses of O₃ to HCHO were positive. However, the HCHO concentration (shown in Figure S13) was lower in central PRD in 2013 than that in 2010, and, therefore, the responses of O₃ to HCHO were negative, while the HCHO concentration was lower in the other regions of the PRD, except the central part, in 2013 than that in 2010, but the responses of O₃ to HCHO were positive.

Moreover, the amplitude of the response of O₃ pollution to SO_X is the second largest among all precursors, with O₃ response values to SO_X lower than -3 $\mu\text{g m}^{-3}$ in southern PRD in 2011. This may be due to the positive feedback of O₃ pollution on SO_X. SO_X concentrations decreased between 2011 and 2020 and were higher in 2011–2014 than that in 2010 (shown in Figure S14), and, therefore, the response values of O₃ to SO_X in 2011–2014 were positive, while SO_X concentrations were lower in 2015–2020 than that in 2010, and, therefore, values of the O₃ response to SO_X in 2015–2020 were negative.

For NO₂, the response value of O₃ pollution to NO₂ in the main region of the PRD decreased from 2011 to 2016, reached a minimum value in 2016, and then increased from 2016 to 2020. This may be related to the different response patterns of O₃ pollution to NO₂ in the PRD [64,65]. The response of O₃ to NO₂ was likely due to negative feedback in 2011–2013, while the response of O₃ to NO₂ was likely due to positive feedback in central PRD from 2014 to 2020. However, the response of O₃ to NO₂ was likely due to positive feedback in northeastern PRD in 2014–2015 and 2017–2020, while the response of O₃ to NO₂ was likely due to negative feedback in this region in 2016. In addition, the response of O₃ to NO₂ was likely due to negative feedback in northwestern PRD in 2014–2020, while the response of O₃ to NO₂ was likely due to positive feedback in southwestern PRD from 2015 to 2020. However, the response of O₃ to NO₂ was likely due to negative feedback in southwestern PRD in 2014. The NO₂ concentration in 2011–2013 was relatively lower than that in 2010, and the response value of O₃ to NO₂ was positive (shown in Figure S12), while the NO₂ concentration in central PRD was higher during 2014–2020 than that in 2010, so the response value of O₃ to NO₂ was positive. Moreover, the NO₂ concentration in northeastern PRD was relatively higher than that in 2010, so the response value of O₃

to NO_2 was positive, while the NO_2 concentration was relatively higher in this region in 2016 than that in 2010, but the response value of O_3 to NO_2 was negative in 2016. The NO_2 concentration was relatively higher in northwestern PRD in 2014–2020 than that in 2010, but the response value of O_3 to NO_2 in 2014–2020 was negative, while the NO_2 concentration was relatively lower in southwestern PRD during 2015–2020 than that in 2010, and the response value of O_3 to NO_2 was negative. However, the NO_2 concentration was relatively higher in southwestern PRD than that in 2010, and the response value of O_3 to NO_2 was negative in this region from 2015 to 2020.

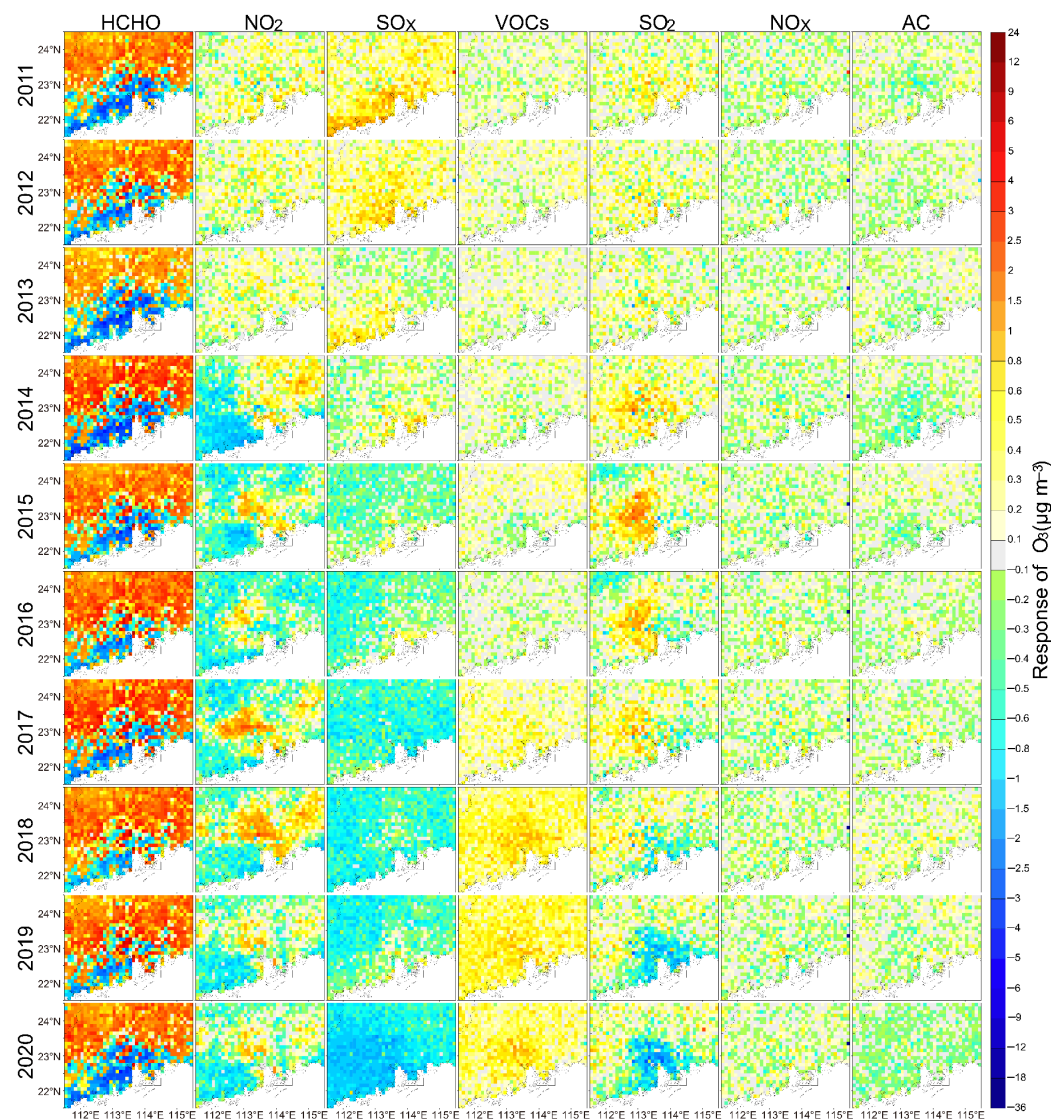


Figure 10. The annual spatial distribution of the response of O_3 pollution to each precursor in the PRD during 2011–2020.

For SO_2 , the response value of O_3 pollution to SO_2 in the main region of the PRD increased from 2011 to 2015, reached the peak value in 2015, and then decreased from 2016 to 2020. This may be due to the different response patterns of O_3 pollution to SO_2 . The response of O_3 to SO_2 was likely due to negative feedback in 2012, while the response of O_3 to SO_2 was likely due to positive feedback in 2011 and in 2013–2020. Compared with 2010, SO_2 concentration in 2011 and 2013–2014 in the PRD were relatively higher (shown in Figure S11), so the response value of O_3 to SO_2 in 2011 and 2013–2014 were positive. In 2012, the SO_2 concentration in the PRD was lower than that in 2010, and the values of the O_3 response to SO_2 were negative. In the northwestern part of the PRD, the SO_2 concentration

was larger than that in 2010, but it decreased significantly from 2015 to 2020, and, therefore, values of the O_3 response to SO_2 were all positive in 2015–2020, but the spatial extent covered by positive values gradually decreased. In contrast, the SO_2 concentration in the southeastern part of the PRD was lower than that in 2010, and it decreased significantly from 2015 to 2020, and, therefore, values of the O_3 response to SO_2 were all negative in this period, but the spatial extent covered by negative values gradually increased.

For VOC, the response of O_3 to VOC in the PRD increased from $0.1 \mu g m^{-3}$ in 2011 to $2.0 \mu g m^{-3}$ in 2020. This may be related to the isotropic feedback of O_3 pollution on VOC in the PRD [66–68]. VOC emissions in the PRD increased from 2011 to 2020 and were relatively higher than that in 2010 (shown in Figure S15), and the response value of O_3 pollution to VOC was positive and increased from 2011 to 2020. Compared with these four precursors, the response of O_3 pollution to SO_2 , NO_X , and aerosol components were relatively smaller.

5. Discussion

Most previous studies only explored the impact of the influencing factors on $PM_{2.5}$ pollution [29] or O_3 pollution [16,30], while there are few studies revealing the effects and contributions of the influencing factors on $PM_{2.5}$ and O_3 collaborative pollution simultaneously [31–33]. In addition, statistical models have also been used by few studies to reveal the influence and contribution of influencing factors to $PM_{2.5}$ and O_3 collaborative pollution, with the mainly considered influencing factors being meteorological [10] and precursor [34–36] factors. In this work, the relative importance of precursor emissions, meteorological factors, population density, NDVI, LULC, and other factors on $PM_{2.5}$ and O_3 collaborative pollution in the NCP, the PRD, and the YRD were assessed comprehensively. In addition, few previous studies using statistical models are not able to estimate and reveal the contribution of the same factor to both $PM_{2.5}$ and O_3 simultaneously, and more than one model needs to be built to estimate and reveal the contribution of a particular factor to both $PM_{2.5}$ and O_3 [35,36]. In this work, daily gridded $PM_{2.5}$ and O_3 datasets and their relative influencing factors were utilized to establish the $PM_{2.5}$ and O_3 MTL estimation model. Subsequently, the same MTL model was used to quantitatively reveal the relative importance of each factor to the $PM_{2.5}$ and O_3 collaborative pollution in each region simultaneously. Furthermore, the response of $PM_{2.5}$ and O_3 to each precursor, as well as the most important precursors for $PM_{2.5}$ and O_3 collaborative pollution, in the NCP, the PRD, and the YRD were quantitatively revealed by the $PM_{2.5}$ and O_3 estimation MTL model.

6. Conclusions

In this work, daily gridded $PM_{2.5}$ and O_3 (maximum daily 8 h average ozone, MDA8)-estimated datasets, precursors, meteorological factors, AOD products, population density, NDVI, and LULC from 2010 to 2020 in three typical regions, including the NCP, the YRD, and the PRD, were utilized to establish the $PM_{2.5}$ and O_3 MTL estimation models for three regions. The sample-based validation results indicated that MTL model-estimated $PM_{2.5}$ and O_3 concentrations exhibit a high correlation with surface $PM_{2.5}$ and O_3 measurements in the NCP, the YRD, and the PRD. The prediction accuracy of these three MTL models was high, with R^2 values of these three models ranging from 0.69 to 0.83, and RMSE values ranging from $9.40 \mu g m^{-3}$ to $16.95 \mu g m^{-3}$.

Subsequently, the $PM_{2.5}$ and O_3 estimation MTL models in the NCP, the PRD, and the YRD were used to quantitatively reveal the influence and contribution of each factor to $PM_{2.5}$ and O_3 collaborative pollution simultaneously. For $PM_{2.5}$ and O_3 pollution in these three regions, precursors (including HCHO, six kinds of VOC, aerosol components, SO_2 , NO_2 , SO_X , and NO_X) were revealed to be the most critical of all influencing factors, with their relative importance ranging from 29.99% to 40.65%. Among these precursors, VOC (including HCHO, C_3H_8 , C_5H_8 , CH_4 , H_2O_2 , OH, and PAN) and aerosol components (including BCSM, DUSMASS25, and OCSM) were found to be the most important dominant

precursors for both PM_{2.5} pollution and O₃ pollution, with their relative importance values being larger than 22.66%. In addition to precursors, meteorological factors are the second most important influencing variables on PM_{2.5} and O₃ pollution in these three regions, with their relative importance values ranging from 15.89% to 20.11%. Moreover, there are several factors such as AOD, LULC, NDVI, population, topography, and month that have a strong influence on PM_{2.5} and O₃ pollution for these regions. These results indicate that surface O₃ and PM_{2.5} pollution in these three regions are largely regulated by VOC, aerosol components, SO_X, and NO_X, which means that reducing the emissions of VOC, aerosols, SO_X, and NO_X can effectively reduce the O₃ and PM_{2.5} pollution levels in the NCP, the PRD, and the YRD.

Furthermore, PM_{2.5} and O₃ estimation MTL models were used to quantitatively reveal the response of PM_{2.5} and O₃ to each precursor pollutant in the NCP, the PRD, and the YRD. The results showed that among these seven PM_{2.5} precursor factors, the four influencing factors with the largest PM_{2.5} pollution response in these three regions were SO₂, HCHO, NO₂, and SO_X, which means that the emission reduction in these four precursors is the most effective measure to mitigate PM_{2.5} pollution in the NCP, the PRD, and the YRD. However, the two most crucial precursors of PM_{2.5} are different across these three regions. The two most important influencing factors on PM_{2.5} pollution in the NCP and YRD are SO₂ and HCHO, with 10-year averaged PM_{2.5} response values of 2.64 $\mu\text{g m}^{-3}$ (for SO₂ in the NCP) and 2.01 $\mu\text{g m}^{-3}$ (for SO₂ in the YRD), and 1.71 $\mu\text{g m}^{-3}$ (for HCHO in the NCP) and 0.95 $\mu\text{g m}^{-3}$ (for HCHO in the YRD), respectively. However, the two most important impact factors on PM_{2.5} pollution in the PRD are SO₂ and NO₂, with 10-year averaged PM_{2.5} response values of 1.24 $\mu\text{g m}^{-3}$ and 0.88 $\mu\text{g m}^{-3}$, respectively.

In terms of O₃ pollution, it indicated that HCHO, NO₂, and SO_X were the three influencing factors that had the greatest response from O₃ in these three regions, and their 10-year average O₃ response values were larger than 0.6 $\mu\text{g m}^{-3}$, which means that emission reduction in VOC, NO₂, and SO_X, are the most effective measures to mitigate O₃ pollution in the NCP, the PRD and the YRD. Moreover, the two most crucial precursors of O₃ are different across these three regions. The two most important influencing factors on O₃ pollution in the NCP and the YRD are HCHO and NO₂, with 10-year averaged O₃ response values of 1.00 $\mu\text{g m}^{-3}$ (for HCHO in the NCP) and 2.89 $\mu\text{g m}^{-3}$ (for HCHO in the YRD), and 0.70 $\mu\text{g m}^{-3}$ (for NO₂ in the NCP) and 0.55 $\mu\text{g m}^{-3}$ (for NO₂ in the YRD), respectively. However, the two most important impact factors on O₃ pollution in the PRD are HCHO and SO_X, with 10-year averaged O₃ response values of 1.79 $\mu\text{g m}^{-3}$ and 0.47 $\mu\text{g m}^{-3}$, respectively.

Overall, in the NCP and the YRD, VOC emission reduction is the most important measure to control PM_{2.5} and O₃ collaborative pollution. In addition, SO₂ emission reduction is another critical measure to control PM_{2.5} pollution, while NO₂ emission reduction is another critical measure to control O₃ pollution. For the PRD, NO₂ emission reduction is the most important measure to control PM_{2.5} and O₃ collaborative pollution. In addition, SO₂ and VOC emission reduction is another critical measure to control PM_{2.5} pollution, while VOC emission reduction is another critical measure to control O₃ pollution. Overall, this study provides clues and references for the control of PM_{2.5} and O₃ collaborative pollution in the NCP, the YRD, and the PRD.

Supplementary Materials: The following supporting information can be downloaded at <https://www.mdpi.com/article/10.3390/su16062475/s1>, Figures S1–S21 and Table S1 are listed.

Author Contributions: Conceptualization, M.M. and Y.L.; methodology, M.M., M.L. (Mengnan Liu) and M.L. (Mengjiao Liu); validation, M.M., M.L. (Mengnan Liu), M.L. (Mengjiao Liu), P.F., F.M. and Z.Z.; formal analysis, M.M., F.M., H.X., J.B., Z.Z. and M.L. (Mengjiao Liu); data curation, M.M.; writing—original draft preparation, M.M. and M.L. (Mengnan Liu); writing—review and editing, M.M. and Y.L.; visualization, M.M., M.L. (Mengnan Liu), P.F. and M.L. (Mengjiao Liu); supervision, M.M. and Y.L.; project administration, M.M. and Y.L.; funding acquisition, M.M., F.M., J.B. and H.X. All authors have read and agreed to the published version of the manuscript.

Funding: This work was supported by the National Natural Science Foundation of China (Grant No. 42301382), the Shandong Provincial Natural Science Foundation (Grant No. ZR2021QD034, Grant No. ZR2022YQ36), the Youth Innovation Team Project of Higher School in Shandong Province (Grant No. 2022KJ201, Grant No. 2023KJ121), and the Jinan City and University Integration Development Project (JNSX2023065).

Institutional Review Board Statement: Not applicable.

Informed Consent Statement: Not applicable.

Data Availability Statement: The data utilized in this study were obtained from the work of Bai et al. (2022) [14] and Ma et al. (2023) [17], the MODIS group, and the China Resource and Environmental Science Data Center (CRESDC) for providing DEM and population density data, Yang and Huang (2021) [38] for providing land use and land cover datasets, ECMWF, the Modern-Era Retrospective analysis for Research and Applications version 2 (MERRA-2), and the Copernicus Atmosphere Monitoring Service (CAMS). Data are available from the authors upon request, and with permission from Bai et al. (2022) [14], Ma et al. (2023) [17], Yang and Huang (2021) [38], the MERRA-2 group, the MODIS group, the CRESDC, ECMWF, and CAMS.

Acknowledgments: The authors are grateful to Bai et al. (2022) [14] for providing surface PM_{2.5}, and AOD (<https://doi.org/10.5194/essd-14-907-2022> (accessed on 20 January 2024)) estimation products, Ma et al. (2023) for providing surface O₃, surface NO₂, and surface SO₂ estimation products (<https://doi.org/10.11117/1.JRS.18.012004> (accessed on 20 January 2024)), the MERRA-2 group for providing aerosol component datasets (<https://disc.gsfc.nasa.gov/datasets?project=MERRA-2> (accessed on 20 January 2024)), the MODIS group for providing NDVI data (<https://ladsweb.modaps.eosdis.nasa.gov/search> (accessed on 20 January 2024)), the China Resource and Environmental Science Data Center for providing DEM and population density data (<http://www.resdc.cn/Default.aspx> (accessed on 20 January 2024)), ECMWF for providing ERA5 reanalysis (<https://cds.climate.copernicus.eu/#/search?text=ERA5> (accessed on 20 January 2024)), and the Copernicus Atmosphere Monitoring Service (CAMS, <https://ads.atmosphere.copernicus.eu/cdsapp#!/search?text=CAMS> (accessed on 20 January 2024)) for providing emissions reanalysis data.

Conflicts of Interest: The authors declare no conflicts of interest.

References

1. Zhou, Y.; Chang, F.-J.; Chang, L.-C.; Kao, I.-F.; Wang, Y.-S.; Kang, C.-C. Multi-Output Support Vector Machine for Regional Multi-Step-Ahead PM_{2.5} Forecasting. *Sci. Total Environ.* **2019**, *651*, 230–240. [[CrossRef](#)]
2. Morawska, L.; Zhu, T.; Liu, N.; Amouei Torkmahalleh, M.; De Fatima Andrade, M.; Barratt, B.; Broomandi, P.; Buonanno, G.; Carlos Belalcazar Ceron, L.; Chen, J.; et al. The State of Science on Severe Air Pollution Episodes: Quantitative and Qualitative Analysis. *Environ. Int.* **2021**, *156*, 106732. [[CrossRef](#)] [[PubMed](#)]
3. Zhang, Y.; Shi, T.; Wang, A.-J.; Huang, Q. Air Pollution, Health Shocks and Labor Mobility. *Int. J. Environ. Res. Public Health* **2022**, *19*, 1382. [[CrossRef](#)] [[PubMed](#)]
4. Ma, M.; Liu, M.; Song, X.; Liu, M.; Fan, W.; Wang, Y.; Xing, H.; Meng, F.; Lv, Y. Spatiotemporal Patterns and Quantitative Analysis of Influencing Factors of PM_{2.5} and O₃ Pollution in the North China Plain. *Atmos. Pollut. Res.* **2023**, *15*, 101950. [[CrossRef](#)]
5. Wu, B.; Liu, C.; Zhang, J.; Du, J.; Shi, K. The Multifractal Evaluation of PM_{2.5}-O₃ Coordinated Control Capability in China. *Ecol. Indic.* **2021**, *129*, 107877. [[CrossRef](#)]
6. Wang, L.; Li, M.; Wang, Q.; Li, Y.; Xin, J.; Tang, X.; Du, W.; Song, T.; Li, T.; Sun, Y.; et al. Air Stagnation in China: Spatiotemporal Variability and Differing Impact on PM_{2.5} and O₃ during 2013–2018. *Sci. Total Environ.* **2022**, *819*, 152778. [[CrossRef](#)]
7. Qi, L.; Zheng, H.; Ding, D.; Ye, D.; Wang, S. Effects of Meteorology Changes on Inter-Annual Variations of Aerosol Optical Depth and Surface PM_{2.5} in China—Implications for PM_{2.5} Remote Sensing. *Remote Sens.* **2022**, *14*, 2762. [[CrossRef](#)]
8. Ho, K.-F.; Lee, Y.-C.; Niu, X.; Xu, H.; Zhang, R.; Cao, J.-J.; Tsai, C.-Y.; Hsiao, T.-C.; Chuang, H.-C. Organic Carbon and Acidic Ions in PM_{2.5} Contributed to Particle Bioreactivity in Chinese Megacities during Haze Episodes. *Environ. Sci. Pollut. Res.* **2022**, *29*, 11865–11873. [[CrossRef](#)]
9. Hu, J.; Zhou, R.; Ding, R.; Ye, D.-W.; Su, Y. Effect of PM_{2.5} Air Pollution on the Global Burden of Lower Respiratory Infections, 1990–2019: A Systematic Analysis from the Global Burden of Disease Study 2019. *J. Hazard. Mater.* **2023**, *459*, 132215. [[CrossRef](#)]
10. Chen, D.; Sandler, D.P.; Keil, A.P.; Heiss, G.; Whitsel, E.A.; Pratt, G.C.; Stewart, P.A.; Stenzel, M.R.; Groth, C.P.; Banerjee, S.; et al. Fine Particulate Matter and Incident Coronary Heart Disease Events up to 10 Years of Follow-up among Deepwater Horizon Oil Spill Workers. *Environ. Res.* **2023**, *217*, 114841. [[CrossRef](#)] [[PubMed](#)]
11. Chen, Z.; Liu, P.; Xia, X.; Wang, L.; Li, X. The Underlying Mechanism of PM_{2.5}-Induced Ischemic Stroke. *Environ. Pollut.* **2022**, *310*, 119827. [[CrossRef](#)]

12. Chuang, M.-T.; Chou, C.C.-K.; Lin, C.-Y.; Lee, J.-H.; Lin, W.-C.; Chen, Y.-Y.; Chang, C.-C.; Lee, C.-T.; Kong, S.S.-K.; Lin, T.-H. A Numerical Study of Reducing the Concentration of O₃ and PM_{2.5} Simultaneously in Taiwan. *J. Environ. Manag.* **2022**, *318*, 115614. [[CrossRef](#)] [[PubMed](#)]
13. Bai, K.; Ma, M.; Chang, N.B.; Gao, W. Spatiotemporal trend analysis for fine particulate matter concentrations in China using high-resolution satellite-derived and ground-measured PM_{2.5} data. *J. Environ. Manag.* **2019**, *233*, 530–542. [[CrossRef](#)] [[PubMed](#)]
14. Bai, K.; Li, K.; Ma, M.; Li, K.; Li, Z.; Guo, J.; Chang, N.-B.; Tan, Z.; Han, D. LGHAP: The Long-Term Gap-Free High-Resolution Air Pollutant Concentration Dataset, Derived via Tensor-Flow-Based Multimodal Data Fusion. *Earth Syst. Sci. Data* **2022**, *14*, 907–927. [[CrossRef](#)]
15. Ma, M.; Bai, K.; Qiao, F.; Shi, R.; Gao, W. Quantifying impacts of crop residue burning in the North China Plain on summertime tropospheric ozone over East Asia. *Atmos. Environ.* **2018**, *194*, 14–30. [[CrossRef](#)]
16. Ma, M.; Yao, G.; Guo, J.; Bai, K. Distinct spatiotemporal variation patterns of surface ozone in China due to diverse influential factors. *J. Environ. Manag.* **2021**, *288*, 112368. [[CrossRef](#)] [[PubMed](#)]
17. Ma, M.; Liu, M.; Liu, M.; Li, K.; Xing, H.; Meng, F. Resolving contributions of NO₂ and SO₂ to PM_{2.5} and O₃ pollutions in the North China Plain via multi-task learning. *J. Appl. Remote Sens.* **2023**, *18*, 012004. [[CrossRef](#)]
18. Yang, J.; Chen, X.; Li, M.; Yao, Q.; Lv, Q.; Gao, B.; Chen, Z. The Division of PM_{2.5}-O₃ Composite Airborne Pollution across China Based on Spatiotemporal Clustering. *J. Clean. Prod.* **2023**, *401*, 136706. [[CrossRef](#)]
19. Zhao, H.; Zhang, Y.; Qi, Q.; Zhang, H. Evaluating the Impacts of Ground-Level O₃ on Crops in China. *Curr. Pollut. Rep.* **2021**, *7*, 565–578. [[CrossRef](#)]
20. Xu, B.; Wang, T.; Gao, L.; Ma, D.; Song, R.; Zhao, J.; Yang, X.; Li, S.; Zhuang, B.; Li, M.; et al. Impacts of Meteorological Factors and Ozone Variation on Crop Yields in China Concerning Carbon Neutrality Objectives in 2060. *Environ. Pollut.* **2023**, *317*, 120715. [[CrossRef](#)]
21. Shen, L.; Zhao, T.; Liu, J.; Wang, H.; Bai, Y. Meteorological Impacts on Interannual Anomalies of O₃ Import over Twain-Hu Basin. *Sci. Total Environ.* **2023**, *888*, 164065. [[CrossRef](#)] [[PubMed](#)]
22. Cao, Y.; Zhao, X.; Su, D.; Cheng, X.; Ren, H. A Machine-Learning-Based Classification Method for Meteorological Conditions of Ozone Pollution. *Aerosol Air Qual. Res.* **2023**, *23*, 220239. [[CrossRef](#)]
23. Sicard, P.; Khaniabadi, Y.O.; Perez, S.; Gualtieri, M.; De Marco, A. Effect of O₃, PM₁₀ and PM_{2.5} on Cardiovascular and Respiratory Diseases in Cities of France, Iran and Italy. *Environ. Sci. Pollut. Res.* **2019**, *26*, 32645–32665. [[CrossRef](#)] [[PubMed](#)]
24. Hu, J.; Chen, G.; Li, S.; Guo, Y.; Duan, J.; Sun, Z. Association of Long-Term Exposure to Ambient Air Pollutants with Cardiac Structure and Cardiovascular Function in Chinese Adults. *Ecotoxicol. Environ. Saf.* **2023**, *249*, 114382. [[CrossRef](#)]
25. Liu, Y.; Geng, G.; Cheng, J.; Liu, Y.; Xiao, Q.; Liu, L.; Shi, Q.; Tong, D.; He, K.; Zhang, Q. Drivers of Increasing Ozone during the Two Phases of Clean Air Actions in China 2013–2020. *Environ. Sci. Technol.* **2023**, *57*, 8954–8964. [[CrossRef](#)]
26. Han, H.; Liu, J.; Shu, L.; Wang, T.; Yuan, H. Local and Synoptic Meteorological Influences on Daily Variability in Summertime Surface Ozone in Eastern China. *Atmos. Chem. Phys.* **2020**, *20*, 203–222. [[CrossRef](#)]
27. An, J.; Shi, Y.; Wang, J.; Zhu, B. Temporal Variations of O₃ and NO_x in the Urban Background Atmosphere of Nanjing, East China. *Arch. Environ. Contam. Toxicol.* **2016**, *71*, 224–234. [[CrossRef](#)]
28. Dong, Z. Synergetic PM_{2.5} and O₃ Control Strategy for the Yangtze River Delta, China. *J. Environ. Sci.* **2023**, *123*, 281–291. [[CrossRef](#)]
29. Wei, J.; Li, Z.; Cribb, M.; Huang, W.; Xue, W.; Sun, L.; Guo, J.; Peng, Y. Improved 1 km resolution PM_{2.5} estimates across China using enhanced space–Time extremely randomized trees. *Atmos. Chem. Phys.* **2020**, *20*, 3273–3289. [[CrossRef](#)]
30. Ou, S.; Wei, W.; Cheng, S.; Cai, B. Exploring drivers of the aggravated surface O₃ over North China Plain in summer of 2015–2019: Aerosols, precursors, and meteorology. *J. Environ. Sci.* **2023**, *127*, 453–464. [[CrossRef](#)]
31. Li, K.; Jacob, D.J.; Liao, H.; Zhu, J.; Shah, V.; Shen, L.; Bates, K.H.; Zhang, Q.; Zhai, S. A two-pollutant strategy for improving ozone and particulate air quality in China. *Nat. Geosci.* **2019**, *12*, 906–910. [[CrossRef](#)]
32. Wang, P.; Guo, H.; Hu, J.; Kota, S.H.; Ying, Q.; Zhang, H. Responses of PM_{2.5} and O₃ Concentrations to Changes of Meteorology and Emissions in China. *Sci. Total Environ.* **2019**, *662*, 297–306. [[CrossRef](#)] [[PubMed](#)]
33. Duan, W.; Wang, X.; Cheng, S.; Wang, R.; Zhu, J. Influencing Factors of PM_{2.5} and O₃ from 2016 to 2020 Based on DLNM and WRF-CMAQ. *Environ. Pollut.* **2021**, *285*, 117512. [[CrossRef](#)]
34. Gong, S.; Zhang, L.; Liu, C.; Lu, S.; Pan, W.; Zhang, Y. Multi-Scale Analysis of the Impacts of Meteorology and Emissions on PM_{2.5} and O₃ Trends at Various Regions in China from 2013 to 2020 2. Key Weather Elements and Emissions. *Sci. Total Environ.* **2022**, *824*, 153847. [[CrossRef](#)]
35. Xu, T.; Zhang, C.; Liu, C.; Hu, Q. Variability of PM_{2.5} and O₃ Concentrations and Their Driving Forces over Chinese Megacities during 2018–2020. *J. Environ. Sci.* **2023**, *124*, 1–10. [[CrossRef](#)]
36. Duan, W.; Wang, X.; Cheng, S.; Wang, R. Regional Collaboration to Simultaneously Mitigate PM_{2.5} and O₃ Pollution in Beijing-Tianjin-Hebei and the Surrounding Area: Multi-Model Synthesis from Multiple Data Sources. *Sci. Total Environ.* **2022**, *820*, 153309. [[CrossRef](#)]
37. Zhang, L.; Zhao, N.; Zhang, W.; Wilson, J.P. Changes in Long-Term PM_{2.5} Pollution in the Urban and Suburban Areas of China's Three Largest Urban Agglomerations from 2000 to 2020. *Remote Sens.* **2022**, *14*, 1716. [[CrossRef](#)]
38. Yang, J.; Huang, X. The 30 m Annual Land Cover Dataset and Its Dynamics in China from 1990 to 2019. *Earth Syst. Sci. Data* **2021**, *13*, 3907–3925. [[CrossRef](#)]

39. Yan, X.; Zuo, C.; Li, Z.; Chen, H.W.; Jiang, Y.; He, B.; Liu, H.; Chen, J.; Shi, W. Cooperative Simultaneous Inversion of Satellite-Based Real-Time PM_{2.5} and Ozone Levels Using an Improved Deep Learning Model with Attention Mechanism. *Environ. Pollut.* **2023**, *327*, 121509. [\[CrossRef\]](#)
40. Ma, X.; Longley, I.; Gao, J.; Salmond, J. Evaluating the Effect of Ambient Concentrations, Route Choices, and Environmental (in)Justice on Students' Dose of Ambient NO₂ while Walking to School at Population Scales. *Environ. Sci. Technol.* **2020**, *54*, 12908–12919. [\[CrossRef\]](#) [\[PubMed\]](#)
41. Mei, B.; Xu, Y. Multi-Task Least Squares Twin Support Vector Machine for Classification. *Neurocomputing* **2019**, *338*, 26–33. [\[CrossRef\]](#)
42. Zhang, Y.; Yang, Q. A Survey on Multi-Task Learning. *IEEE Trans. Knowl. Data Eng.* **2022**, *34*, 5586–5609. [\[CrossRef\]](#)
43. Zhang, Y.; Yang, Q. An Overview of Multi-Task Learning. *Natl. Sci. Rev.* **2018**, *5*, 30–43. [\[CrossRef\]](#)
44. Vafaeikia, P.; Namdar, K.; Khalvati, F. A Brief Review of Deep Multi-Task Learning and Auxiliary Task Learning. *arXiv* **2020**, arXiv:2007.01126.
45. Yang, Q.; Yuan, Q.; Gao, M.; Li, T. A New Perspective to Satellite-Based Retrieval of Ground-Level Air Pollution: Simultaneous Estimation of Multiple Pollutants Based on Physics-Informed Multi-Task Learning. *Sci. Total Environ.* **2023**, *857*, 159542. [\[CrossRef\]](#)
46. Wu, X.; Xin, J.; Zhang, W.; Gao, W.; Ma, Y.; Ma, Y.; Wen, T.; Liu, Z.; Hu, B.; Wang, Y.; et al. Variation Characteristics of Air Combined Pollution in Beijing City. *Atmos. Res.* **2022**, *274*, 106197. [\[CrossRef\]](#)
47. Yang, X.; Wang, L.; Ma, P.; He, Y.; Zhao, C.; Zhao, W. Urban and Suburban Decadal Variations in Air Pollution of Beijing and Its Meteorological Drivers. *Environ. Int.* **2023**, *181*, 108301. [\[CrossRef\]](#)
48. Zhang, L.; An, J.; Liu, M.; Li, Z.; Liu, Y.; Tao, L.; Liu, X.; Zhang, F.; Zheng, D.; Gao, Q.; et al. Spatiotemporal Variations and Influencing Factors of PM_{2.5} Concentrations in Beijing, China. *Environ. Pollut.* **2020**, *262*, 114276. [\[CrossRef\]](#)
49. Wang, S.; Zhang, Y.; Ma, J.; Zhu, S.; Shen, J.; Wang, P.; Zhang, H. Responses of Decline in Air Pollution and Recovery Associated with COVID-19 Lockdown in the Pearl River Delta. *Sci. Total Environ.* **2021**, *756*, 143868. [\[CrossRef\]](#)
50. Wei, J.; Li, Z.; Li, K.; Dickerson, R.R.; Pinker, R.T.; Wang, J.; Liu, X.; Sun, L.; Xue, W.; Cribb, M. Full-Coverage Mapping and Spatiotemporal Variations of Ground-Level Ozone (O₃) Pollution from 2013 to 2020 across China. *Remote Sens. Environ.* **2022**, *270*, 112775. [\[CrossRef\]](#)
51. Lu, X.; Zhang, L.; Chen, Y.; Zhou, M.; Zheng, B.; Li, K.; Liu, Y.; Lin, J.; Fu, T.-M.; Zhang, Q. Exploring 2016–2017 Surface Ozone Pollution over China: Source Contributions and Meteorological Influences. *Atmos. Chem. Phys.* **2019**, *19*, 8339–8361. [\[CrossRef\]](#)
52. Lin, X.-Y.; Xia, S.-Y.; Luo, Y.; Han, H.-X.; He, L.-Y. Evaluation of Key Factors Influencing Urban Ozone Pollution in the Pearl River Delta and Its Atmospheric Implications. *Atmos. Environ.* **2023**, *305*, 119807. [\[CrossRef\]](#)
53. Liu, Q.; Liu, T.; Chen, Y.; Xu, J.; Gao, W.; Zhang, H.; Yao, Y. Effects of Aerosols on the Surface Ozone Generation via a Study of the Interaction of Ozone and Its Precursors during the Summer in Shanghai, China. *Sci. Total Environ.* **2019**, *675*, 235–246. [\[CrossRef\]](#) [\[PubMed\]](#)
54. Mu, G.; Wang, B.; Yang, S.; Wang, X.; Zhou, M.; Song, W.; Qiu, W.; Ye, Z.; Zhou, Y.; Chen, W. Assessment for Personal PM_{2.5} Exposure with a Modeling Method: A Panel Study in Wuhan, China. *Atmos. Pollut. Res.* **2020**, *11*, 1991–1997. [\[CrossRef\]](#)
55. Zhu, J.; Chen, L.; Liao, H.; Dang, R. Correlations between PM_{2.5} and Ozone over China and Associated Underlying Reasons. *Atmosphere* **2019**, *10*, 352. [\[CrossRef\]](#)
56. Lou, C.; Liu, H.; Li, Y.; Peng, Y.; Wang, J.; Dai, L. Relationships of Relative Humidity with PM_{2.5} and PM10 in the Yangtze River Delta, China. *Environ. Monit. Assess.* **2017**, *189*, 582. [\[CrossRef\]](#)
57. Luo, Y.; Zhao, T.; Yang, Y.; Zong, L.; Kumar, K.R.; Wang, H.; Meng, K.; Zhang, L.; Lu, S.; Xin, Y. Seasonal Changes in the Recent Decline of Combined High PM_{2.5} and O₃ Pollution and Associated Chemical and Meteorological Drivers in the Beijing–Tianjin–Hebei Region, China. *Sci. Total Environ.* **2022**, *838*, 156312. [\[CrossRef\]](#)
58. Gui, K.; Che, H.; Wang, Y.; Wang, H.; Zhang, L.; Zhao, H.; Zheng, Y.; Sun, T.; Zhang, X. Satellite-Derived PM_{2.5} Concentration Trends over Eastern China from 1998 to 2016: Relationships to Emissions and Meteorological Parameters. *Environ. Pollut.* **2019**, *247*, 1125–1133. [\[CrossRef\]](#)
59. Wei, W.; Chen, S.; Wang, Y.; Cheng, L.; Wang, X.; Cheng, S. The Impacts of VOCs on PM_{2.5} Increasing via Their Chemical Losses Estimates: A Case Study in a Typical Industrial City of China. *Atmos. Environ.* **2022**, *273*, 118978. [\[CrossRef\]](#)
60. Zhao, K.; Yuan, Z.; Wu, Y.; Huang, J.; Yang, F.; Zhang, X.; Huang, D.; Jiang, R. Identification of Synergistic Control for Ozone and PM_{2.5} Pollution during a Large-Scale Emission Reduction in China. *Atmos. Res.* **2023**, *295*, 107025. [\[CrossRef\]](#)
61. Meng, Z.; Dabdub, D.; Seinfeld, J.H. Chemical Coupling between Atmospheric Ozone and Particulate Matter. *Science* **1997**, *277*, 116–119. [\[CrossRef\]](#)
62. Chu, B.; Zhang, S.; Liu, J.; Ma, Q.; He, H. Significant Concurrent Decrease in PM_{2.5} and NO₂ Concentrations in China during COVID-19 Epidemic. *J. Environ. Sci.* **2021**, *99*, 346–353. [\[CrossRef\]](#) [\[PubMed\]](#)
63. Li, S.; Liu, N.; Tang, L.; Zhang, F.; Liu, J.; Liu, J. Mutation Test and Multiple-Wavelet Coherence of PM_{2.5} Concentration in Guiyang, China. *Air Qual. Atmos. Health* **2021**, *14*, 955–966. [\[CrossRef\]](#)
64. Wang, Y.; Yang, X.; Wu, K.; Mei, H.; De Smedt, I.; Wang, S.; Fan, J.; Lyu, S.; He, C. Long-Term Trends of Ozone and Precursors from 2013 to 2020 in a Megacity (Chengdu), China: Evidence of Changing Emissions and Chemistry. *Atmos. Res.* **2022**, *278*, 106309. [\[CrossRef\]](#)

65. Li, Y.; Wu, Z.; Ji, Y.; Chen, T.; Li, H.; Gao, R.; Xue, L.; Wang, Y.; Zhao, Y.; Yang, X. Comparison of the Ozone Formation Mechanisms and VOCs Apportionment in Different Ozone Pollution Episodes in Urban Beijing in 2019 and 2020: Insights for Ozone Pollution Control Strategies. *Sci. Total Environ.* **2024**, *908*, 168332. [[CrossRef](#)]
66. Zhang, X.; Ma, Q.; Chu, W.; Ning, M.; Liu, X.; Xiao, F.; Cai, N.; Wu, Z.; Yan, G. Identify the Key Emission Sources for Mitigating Ozone Pollution: A Case Study of Urban Area in the Yangtze River Delta Region, China. *Sci. Total Environ.* **2023**, *892*, 164703. [[CrossRef](#)]
67. Xie, Y.; Cheng, C.; Wang, Z.; Wang, K.; Wang, Y.; Zhang, X.; Li, X.; Ren, L.; Liu, M.; Li, M. Exploration of O₃-Precursor Relationship and Observation-Oriented O₃ Control Strategies in a Non-Provincial Capital City, Southwestern China. *Sci. Total Environ.* **2021**, *800*, 149422. [[CrossRef](#)]
68. Liu, Z.; Hu, K.; Zhang, K.; Zhu, S.; Wang, M.; Li, L. VOCs Sources and Roles in O₃ Formation in the Central Yangtze River Delta Region of China. *Atmos. Environ.* **2023**, *302*, 119755. [[CrossRef](#)]

Disclaimer/Publisher's Note: The statements, opinions and data contained in all publications are solely those of the individual author(s) and contributor(s) and not of MDPI and/or the editor(s). MDPI and/or the editor(s) disclaim responsibility for any injury to people or property resulting from any ideas, methods, instructions or products referred to in the content.